ELSEVIER

Quaternary Science Reviews 25 (2006) 659–688

QSR

A calibrated deglacial drainage chronology for the North American continent: evidence of an Arctic trigger for the Younger Dryas

Lev Tarasov*, W.R. Peltier

Department of Physics, University of Toronto, Toronto, Ont., Canada M5S 1A7

Received 24 April 2005; accepted 18 December 2005

Abstract

We present a new deglacial meltwater drainage chronology for the North American ice-sheet complex using a 3D glacial systems model calibrated against a large set of paleo-proxies. Results indicate that North America was responsible for a significant fraction of mwp1-a, with order 1.5 dSv or larger (100 year mean) peak discharges into both the Gulf of Mexico and the Eastern Atlantic and less than 1 dSv into the Arctic Ocean.

Our most significant result concerns discharge into the Arctic Ocean. The largest total discharge into the Arctic Ocean (ensemble mean values of 1.0–2.2 dSv) occurs during the onset of the Younger Dryas. The large majority of this discharge is locally sourced with reduction of the Keewatin ice dome being the largest contributor. Given that the only outlet from the Arctic Basin at this time was via Fram Strait into the Greenland–Iceland–Norwegian Seas, we hypothesize that this pulse was the trigger for the re-organization of thermohaline circulation that is thought to have been responsible for the Younger Dryas cold interval. In contradistinction with past inferences and subject to the imperfectly constrained ice-margin chronology, we also find that the Northwest outlet likely dominated much of the post −13 ka drainage of Lake Agassiz.

1. Introduction

The deglaciation of the North American continent produced large fluxes of meltwater and icebergs into the adjacent ocean basins, often in the form of abrupt catastrophic events. These events are believed to have significantly influenced the thermohaline circulation of the oceans and therefore northern hemispheric climate. This inference derives in large part from consideration of the two most significant millennial-scale climatic variations that occurred during the deglacial period. The Bolling–Allerod (B–A) warm interval and the subsequent Younger Dryas (YD) cold interval both persisted over periods of order 1 ka and were characterized by fast onsets and terminations. This is evident in the $\delta^{18}O$ time series from the Greenland summit ice cores (Johnsen et al., 2001), which constitute a proxy for the temperature of the air from which precipitation was derived. Given that the deep ocean circulation is the component of the climate system that most clearly operates over this range of time scales, it has become generally accepted that these two dramatic climate events are associated with major changes in the formation of North Atlantic Deep Water (NADW) and thus in the strength of the Meridional Overturning Circulation (MOC) of the oceans. The B–A has been inferred to correspond to a sudden onset of NADW formation after this had been arrested (McManus et al., 2004) due to the freshening of the surface of the North Atlantic caused by iceberg discharge associated with Heinrich event 1 (H1). Conversely, the YD is believed to correspond to a sudden and significant reduction of NADW production due to a later freshening event, the cause of which is uncertain. Various paleo-oceanographic proxies together with the occurrence of a contemporaneous ^{14}C plateau are fully consistent with an interpretation of the YD as a northern hemispheric cooling event triggered by a significant reduction in NADW formation and resultant reorganization of the thermohaline circulation

*Corresponding author. Tel.: +1 519 821 3555; fax: +1 416 978 8905.
E-mail addresses: lev@atmosp.physics.utoronto.ca (L. Tarasov), peltier@atmosp.physics.utoronto.ca (W.R. Peltier).

0277-3791/$ - see front matter © 2006 Elsevier Ltd. All rights reserved.
doi:10.1016/j.quascirev.2005.12.006

(THC) (Keigwin et al., 1991; Hughen et al., 1998; Muscheler et al., 2000; McManus et al., 2004).

In searching for a trigger for the YD, Broecker et al. (1989) (building on the work of Rooth, 1982) initially hypothesized the occurrence of a large "pulse" of meltwater through the St. Lawrence river system associated with the opening of an eastern outlet for Lake Agassiz (Fig. 1). It was suggested that this pulse of freshwater would have been transported as a surface plume through the Gulf of St. Lawrence and out onto the surface of the North Atlantic, thus rendering the region incapable of the convective instability which drives NADW production. However, this suggestion was subsequently found to be in conflict with sea surface salinity reconstructions for the Gulf of St. Lawrence basin, which indicate reduced rather than enhanced surface meltwater flows during the YD (de Vernal et al., 1996). Furthermore, ^{14}C ages of invertebrate fossil assemblages associated with the highest salinity water of the Champlain Sea indicate that freshening of the Champlain Sea (which existed in the St. Lawrence Lowlands, from northeast of Lake Ontario to Quebec City) occurred only subsequent to 10.5 ^{14}C ka before present (^{14}C ka hereafter) (Rodrigues and Vilks, 1994). It is also likely that this 10.5 ^{14}C ka age is too old given the identification of large regional ^{14}C reservoir effects (Richard and Occhietti, 2005). These data along with some recent examinations of possible eastern Lake Agassiz outlets Lowell et al., 2005; Teller et al., 2005 suggest that this outlet was closed during the onset of and possibly throughout the YD. Unambiguous identification of the dynamical "trigger" that was responsible for the reduction in NADW production during the YD has therefore remained elusive.

Our understanding of the role that fresh-water fluxes may play in THC reorganization is further challenged by the apparent lack of response of the MOC to the large flux of meltwater into the oceans that occurred during meltwater pulse 1-a (mwp1-a) when eustatic sea level rose approximately 20 m within a 500 year period (Fairbanks, 1989; Hanebuth et al., 2000). In consideration of this issue, Clark et al. (1996) have argued that the North American ice complex could not therefore have been a major contributor to mwp1-a since this pulse occurred almost simultaneously with the onset of the interglacial mode of

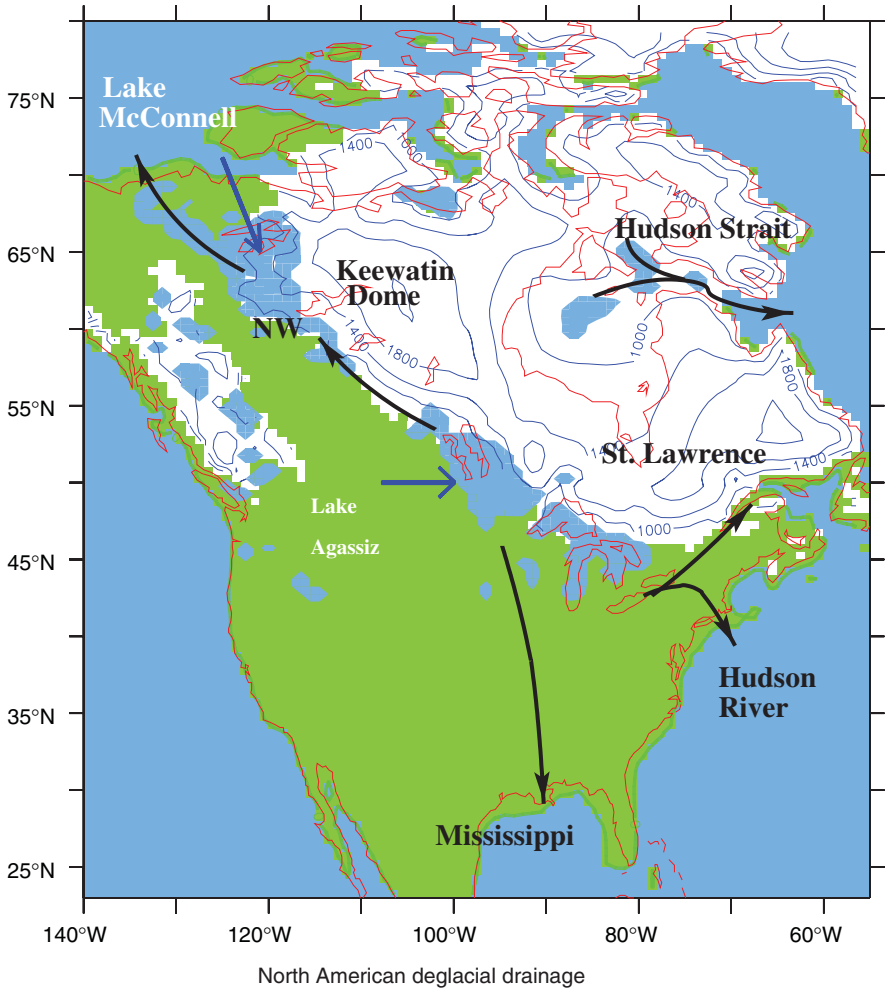

Fig. 1. Major deglacial drainage outlets for North America. The present day coastline is outlined in red. Northwestern drainage is via the Mackenzie River basin (which commences around "NW").

strong thermohaline circulation, which is inferred to have been the cause of the onset of the B–A warm period. Early general circulation model-based analyses (e.g., Manabe and Stouffer, 1997) did seem to indicate that such a large discharge of meltwater onto the surface of the mid-to-North Atlantic would have led to an immediate collapse of NADW formation. However, these analyses were predicated on the assumption that a pulse of meltwater into the Atlantic due to enhanced river runoff would have stayed essentially intact near the surface while being advected to the sites of deepwater production, thus leading to THC collapse. This assumption is, however, questionable on the basis of two lines of argument. First, it relies on the traditional stratified surface plume criterion that the bulk density of the meltwater–sediment mixture lies below that of the ambient ocean water. Recent laboratory experiments, however, indicate that sediment-induced mixing can occur at much lower sediment concentrations than usually assumed. Using a parameter regime similar to temperate riverine observations, Parsons et al. (2001) obtain intense downward mixing of sediment-laden outflow at sediment concentrations as low as $1\,kg/m^3$ that can thereby lead to bottom-riding hyperpycnal meltwater plumes rather than surface freshening. Indeed, new isotopic records of depth-stratified foraminifera from the northern Gulf of Mexico are consistent with hyperpycnal meltwater flows during the mwp1-a event (Aharon, 2006). To the extent that mwp1-a was driven primarily by sediment-laden river outflow through the muddy Mississippi and to a lesser extent Hudson River channels (Fig. 1), one would therefore not expect a significant impact on the MOC. Second, transport of such a freshwater pulse to the high latitudes would be via the western boundary current (the Gulf Stream). However, this current is subject to intense baroclinic instability and therefore to strong turbulent mixing (e.g., Bush et al., 1996). Since non-eddy resolving models of the ocean general circulation such as that employed by Manabe and Stouffer (1997) do not incorporate the influence of this mixing, the predictions of such models cannot provide accurate estimates of the extent to which freshwater input originating from the south might influence the NADW formation process.

These fundamental issues of fluid mechanics strongly undermine the arguments of Clark et al. (1996) in favour of an Antarctic source for mwp1-a. Given the strong correlation between Heinrich events and THC shutdown, it would furthermore appear that a significant MOC response is to be expected only when meltwater is directly added to the surface of the ocean, where deep convection would otherwise occur (e.g., entailing transport of freshwater as icebergs directly onto the NADW formation region).

A further challenge to our understanding of the impact of meltwater floods on NADW formation has been raised in connection with the work of Lohmann and Schulz (2000), which suggests that the poor representation of deepwater flow over the Greenland–Scotland ridge artificially increases ocean circulation model sensitivity to deglacial meltwater fluxes that are injected directly into the North Atlantic (or Gulf of Mexico). On the other hand, a strong injection of meltwater and icebergs into the Arctic basin and a resultant expected increase of sea-ice flux into the Greenland–Icelandic–Norwegian (GIN) Seas region would likely have a much stronger impact on deep-water formation. This could also explain the strength of the YD cold interval that occurred relatively late in the deglaciation process. Indeed the operation of such a mechanism has already been hypothesized for the Preboreal climatic oscillation that occurred just after the termination of the YD. Fisher et al. (2002) and Teller et al. (2002) have argued that the opening of a Northwest (NW) outlet for Lake Agassiz was coincident with the onset of the Preboreal oscillation, and that this oscillation was the result of a large flux of meltwater and sea-ice into the Arctic basin.

A possible Arctic basin meltwater trigger for the YD was previously suggested by Bauch et al. (2001) based upon an observed (though represented by only a single data-point) sharp reduction in planktonic $\delta^{18}O$ in the PS1230 core from western Fram Strait (bracketed between 10.5 ^{14}C ka and 12.8 ^{14}C ka) along with the absence of such a signal in Nordic sea cores such as PS1243 from the central GIN sea region. This datum together with three further planktonic $\delta^{18}O$ data-points from 2 other sedimentary cores (PS2837, PS2887) in western Fram Strait (Norgaard-Pedersen et al., 2003) collectively appear to indicate the presence of a strong Arctic freshening event between 10.5 and 11.2 ^{14}C ka (bracketing YD onset). The PS1243 $\delta^{13}C$ record also indicates a slowdown of vertical convection (and thus likely reduced NADW formation) near the beginning of the YD. However, as a reminder of conceptual and observational uncertainties, it should be noted that data from this latter core appear to indicate strong vertical convection during the early middle of the YD.

The possibility of significant meltwater flux through the Canadian Arctic and into the Arctic Ocean during the onset of the YD has however received scant attention. To date, it has been widely assumed that Lake Agassiz drained to the east during the beginning of the YD (Clark et al., 2001; Teller, 2002; Teller et al., 2002; Dyke, 2004) despite the above mentioned contradictory evidence from the St. Lawrence basin. Furthermore, on the basis of both geomorphology (Dyke and Prest, 1987) and geodetic observations (Peltier, 2002, 2004; Tarasov and Peltier, 2004), a large Keewatin ice dome is inferred to have existed during the late glacial and/or early deglacial period. The deglaciation of the region covered by this dome would have produced large fluxes of meltwater. As such, with or without Lake Agassiz drainage influx, significant meltwater discharge from the NW sector of the Laurentide ice-sheet into the Arctic basin (Fig. 1) becomes a hypothesis worth testing.

Direct evidence for meltwater discharge into the Canadian sector of the Arctic Ocean is limited. Poore

et al. (1999) provide clear evidence for significant variations in sea-surface salinity and ice cover during the mwp1-a to YD interval from three box cores extracted from the Mendeleyev Ridge in the western Arctic Ocean. One of the cores (94 B-16) shows strong surface freshening during the YD onset period. However, low sedimentation rates, bioturbation, and weak chronological correlations across the three cores leaves the exact chronology unclear.

Given the lack of significant direct evidence for or against substantial Arctic freshwater discharge during YD onset, reconstructions of Laurentide deglacial surface drainage offer an arguably more direct approach to resolving the issue. Previous reconstructions of Laurentide surface meltwater routing have been largely based on geographically limited field data in combination with isobase maps, which are poorly constrained over the interior NW quadrant of continental Canada (and to a lesser though not insignificant extent they are problematic in the Lake Agassiz basin region where the chronology of lake levels is poorly known). In this regard, the work of Leverington et al. (2002) and Teller and Leverington (2004) represents the most rigorous attempts to date. The limitations of this approach are clear given the differences in interpretation that have occurred. For instance, until the early 1990s, no significant consideration was given to the possible existence of a NW outlet for Lake Agassiz. Subsequently, evidence for a NW outlet during the time of the Preboreal oscillation has been forthcoming (Smith and Fisher, 1993; Fisher and Smith, 1994). Furthermore, this approach is limited to snapshots of surface drainage routing. And given the lack of coupling to a constrained ice-sheet model (ISM) lacks a self-consistent method for computing a chronology of meltwater fluxes from the ice sheets.

In this paper, expanding on Tarasov and Peltier (2005), we offer an independent and complementary analysis of surface drainage for North American (NA) deglaciation using a dynamical 3D thermo-mechanically coupled ISM that incorporates an accurate accounting of visco-elastic bedrock response as well as a fast meltwater routing/storage solver. This approach provides a physically integrated and dynamically self-consistent analysis of the meltwater routing and discharge issues. Bayesian calibration of the model together with the application of forcing at the ice-margins constrained by a newly available high-resolution margin chronology (Dyke et al., 2003; Dyke, 2004) provides strong constraints on the results of the ensemble-based analyses as well as an estimate of the range of models capable of satisfying the observations. Furthermore, detailed comparisons of computed NW and eastern outlet choke-point elevations will allow assessment of the confidence in the derived meltwater routing history. As such, the work presented herein represents a much more highly constrained analysis of deglacial drainage than the earlier dynamical model-based analyses of Marshall and Clarke (1999). In what follows, a brief description of the model precedes a presentation of model results and a discussion of the implications of the revised drainage chronology insofar as expected climate impacts are concerned. Our conclusions are summarized in Section 5.

2. The University of Toronto Glacial Systems Model

The University of Toronto Glacial Systems Model (GSM) incorporates a number of interacting components including: a 3D thermo-mechanically coupled ISM that includes a model of sub-surface thermal evolution, a representation of fast flow due to subglacial till-deformation, a model of visco-elastic bedrock response, a surface mass-balance module, an ice calving module, and finally a fast dynamical meltwater surface routing and storage solver. The ISM uses the standard shallow-ice approximation for ice dynamics and the Glen flow law for ice rheology. Grid resolution for the analyses to be presented herein is 1° longitude by 0.5° latitude. We use an ice flow enhancement factor of 6.0, selected on the basis of our best-fit dynamical models for the Greenland Ice Sheet (Tarasov and Peltier, 2002, 2003).

The ice sheet and bed thermal modules are based on a finite volume discretization of the conservation of energy relation and account for vertical heat conduction, 3D heat advection (in ice), deformation heating, and heating due to basal motion. The deep geothermal heat flux is taken from the digital map of Pollack et al. (1993). The thermo-mechanical ISM has been verified against other comparable models in the EISMINT II model intercomparison project (Payne et al., 2000; Tarasov and Peltier, 2002). The model has been fully described in previous publications (Tarasov and Peltier, 1999, 2002, 2004) and so only an abbreviated discussion will be presented herein.

The bedrock response component of the GSM is based on the linear visco-elastic field theory for a spherically symmetric Maxwell model of the Earth developed in earlier work (Peltier, 1974, 1976). It employs the VM2 radial viscosity profile (Peltier, 1996; Peltier and Jiang, 1996) with a 100 km thick surface lithosphere in which the viscosity is assumed to be infinite. The PREM model (Dziewonski and Anderson, 1981) is taken to define the radial elastic component of the structure. Bedrock response is computed spectrally using the methodology described in Peltier (1976) with truncation at degree and order 256. The visco-elastic model of the glacial isostatic adjustment process is coupled asynchronously to the ISM using a 100 year time-step. For the coupled model (but not for the relative sea level (RSL) calculations that are required to compare model predictions to these observations) an eustatic approximation is invoked to compute the contribution to the surface mass load due to changing sea level. Post-LGM load changes due to the variation of lake levels are also included in the calculation. Isostatic equilibrium is assumed at the time of model initialization at -122 ka (during the Eemian period, i.e. the time of the last interglacial) using a map of present day topography recursively corrected with present day topographic anomalies from early well-calibrated model

runs so as to produce a close match to present day topography after a transient run. In order to calibrate the large ensemble of model runs, RSL histories are computed off-line using the full gravitationally self-consistent theory of post glacial sea level change most recently reviewed in Peltier (1998, 2004). Details of the design of the large ensemble analyses are provided in Tarasov and Peltier (2004).

The surface mass-balance component of the model employs a positive-degree day methodology with temperature-dependent coefficients in order to compute ice and snow ablation as described in Tarasov and Peltier (2002). Rain–snow fractions are computed using a normal statistical model to represent daily and diurnal variations in surface temperature. Any parameter uncertainties in the surface mass-balance are assumed to be absorbed into the climate forcing ensemble parameters described below.

When the basal temperature approaches the pressure melting point, basal sliding and/or basal till-deformation are smoothly activated. Basal sliding is computed using an exponent 3 sliding law with a moderate sliding parameter. When sufficient sub-glacial till is present according to a sediment map derived from the sediment thickness map of Laske and Masters (1997) and the surficial geology map of Fulton (1995), visco-plastic till deformation is assumed. Till viscosity is taken to be an ensemble parameter while remaining till deformation model parameters are taken from Jenson et al. (1996). Ice-shelves are also crudely modelled by the imposition of fast linear sliding upon flotation.

The ice-calving module accounts for both buoyancy effects and ice blockage of drainage channels and incorporates explicit temperature dependence. Given the poor constraints on calving dynamics, three ensemble parameters are assigned to the calving model. The coupled model (but not the off-line RSL calculation) is forced using the SPECMAP δ^{18}O (Imbrie et al., 1984) chronology for eustatic sea-level variations assuming a maximum drop at LGM that is consistent with the Barbados record (Fairbanks, 1989).

The two remaining components of the GSM (climate forcing and drainage solver) are new and are described in the following subsections.

2.1. Drainage solver

Our diagnostic drainage solver is based on a depression-fill and down-slope flow drainage algorithm but with additional analysis at each time-step that includes the computation of inland lake levels. The first pass of the algorithm determines down-slope drainage pointers for each grid-cell. These pointers are set to the nearest downslope drainage collection points which are either inland lakes (i.e. topographic depressions) or deep-water outlets (grid-cells with present day bathymetry (below 600 m)). The first pass also determines maximum fill levels for all inland depressions beyond which overflow occurs. This second pass of the algorithm repeats the downslope drainage calculation but with depression (lake) fill levels now limited by mass conservation (i.e. drainage input plus stored water from the previous time-step) and the over-flow fill level from the first pass. Drainage pointers are updated as lakes are filled. The meltwater discharge into each oceanic drainage basin then follows from summation of total discharge into the deep-water outlets in each basin. For drainage algorithm verification, mass conservation between meltwater inputs and deepwater outlets after accounting for water storage has been monitored and is always maintained. Furthermore, extensive examination of topographic time-slices from selected model runs have been used to directly verify the accuracy of the computed drainage routing.

Drainage routing and proglacial lake levels are computed every 100 years. Total glacial surface discharge (i.e. meltwater and icebergs) are lumped together. The drainage solver includes numerous diagnostics such as dynamic identification of choke-points controlling Lake Agassiz drainage. The algorithm is fast, thus enabling its incorporation into ongoing large ensemble modelling of NA ice complex deglaciation. However, results from the drainage solver are subject to the following caveats. First, a difficult to avoid limitation of paleo drainage modelling is the lack of accounting for surface erosion. Our base ensembles assume past topographic changes due to surface erosion or sediment dams at only the Southern Outlet (SO) choke-point for southern drainage of Lake Agassiz as detailed below. Second, the drainage model uses surface slopes only and therefore does not allow for sub-glacial drainage. Third, it should be underlined that our drainage results represent 100 year mean values. Actual meltwater discharge likely had strong sub 100 year variability as sediment dams broke, ice streams surged, and choke-points opened up. Fourth, the algorithm assumes 0 water depth across controlling sills. Fifth, groundwater infiltration is ignored. Finally, perturbations of the geoid are not computed in the coupled model and as such, lake levels directly adjacent to the ice sheet are somewhat underestimated while those more distal will tend to be slightly over-estimated. The importance of the latter effect will be investigated in later work.

Critical to accurate drainage determination is the modelled surface topography with respect to the modern geoid (i.e. sea level), especially in the context of relatively low spatial resolution drainage modelling. The ISM surface topography is used for ice covered regions. For ice-free regions, we have derived a surface topography from the HYDRO1k hydrologically correct DEM (http://edcdaac.usgs.gov/gtopo30/hydro/na_dem.html) shown in Fig. 2a, which was in turn derived from the gtopo30 DEM. The Terrain-Base DEM (http://www.ngdc.noaa.gov/seg/fliers/se-1104.shtml) provides bathymetry. A base coarse-graining of HYDRO1k was obtained by choosing the lowest sub-grid elevation (“control point”) that met the following two requirements: (1) the number of sub-grid points with

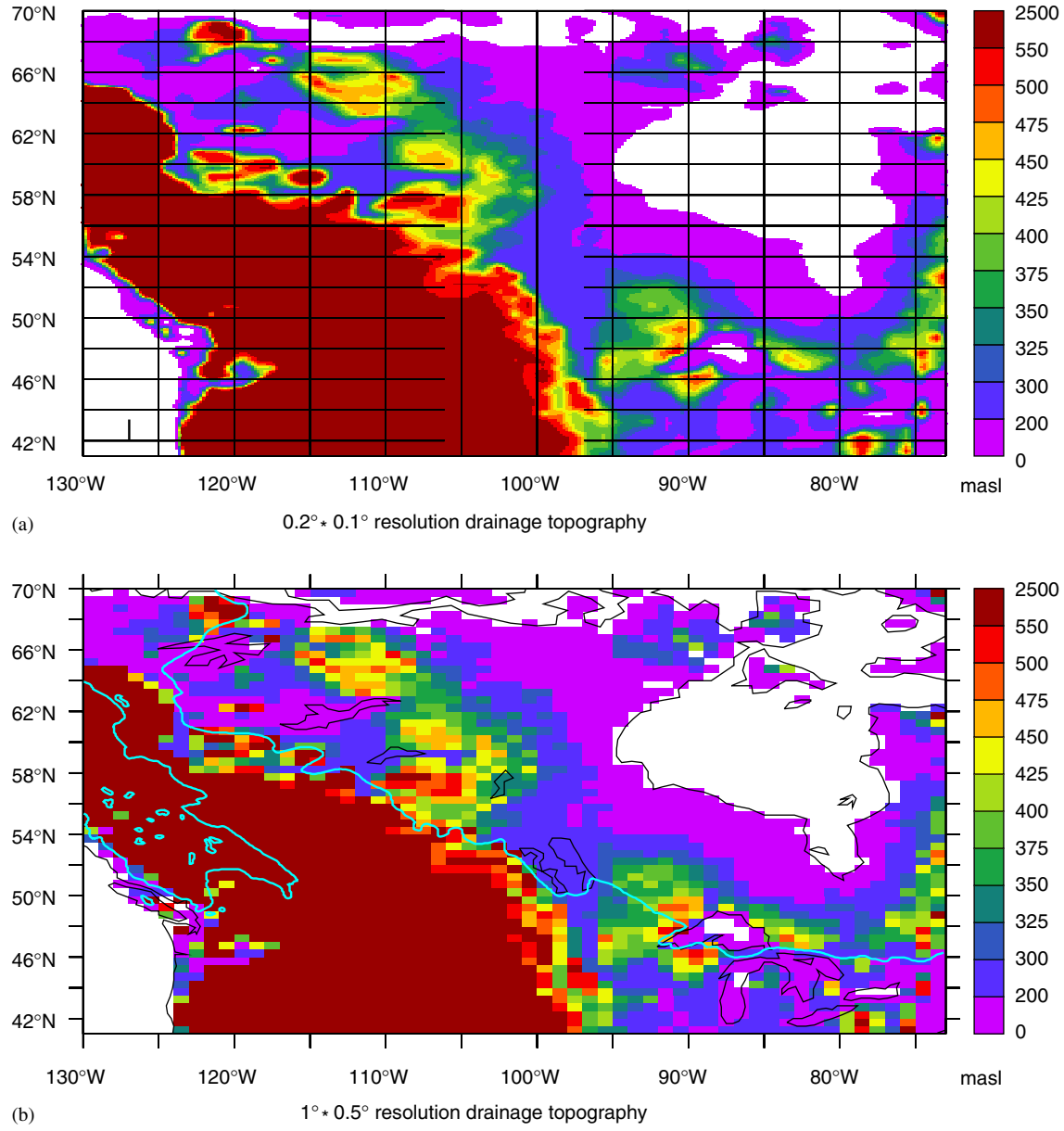

Fig. 2. Drainage topographies. Shown are geographically restricted views of a coarsened version of the HYDRO1k DEM "(a)" and the MDhby 1° longitude *0.5° latitude topography "(b)" used in the drainage solver. Also shown in (b) are the −13 ka (light blue) and −10.2 ka (red) high-resolution ice margins.

elevation less than or equal to that of the control point is adequate to span the grid-cell, (2) this spanning subset must either include points from two different edges or must cross a centre axis of the grid-cell while including two points from the same edge.

However, this initial map required considerable additional work involving cell by cell corrections in critical drainage control regions (choke-points) along with adjustments to match present day Great Lakes volumes. The final version (MDhby) employed in the drainage solver is shown in Fig. 2b. The isostatic visco-elastic response of the Earth's surface to ice and water loads is also added to the drainage topography. As a test of the drainage topography, after construction, the topography was compared against published eastern Lake Agassiz outlet (Nipigon basin) sill elevations (Teller and Thorleifson, 1983). The drainage topography had elevations within 1 m of the lowest sill in two of the covering grid-cells and within 6 m for the remaining covering grid-cell.

The combined coarse-grid drainage topography and drainage solver has also been verified against a coarse-grained version of the level 1 drainage basins of the HYDRO1k data-set derived using a GIS-based surface drainage solver applied to the high-resolution DEM. Drainage basin boundaries are visually in close agreement (not shown). As a concrete example, the difference in

computed Mackenzie basin discharge (using the GSM present day precipitation field modified for elevation effects) is 1% while the drainage basin area difference is 3%. However, there is a 34% excess in the computed discharge as compared to the 0.11 dSv ($\mathrm{dSv} = 10^5\,\mathrm{m}^3/\mathrm{s}$) estimate of Aagaard and Carmack (1989). Even larger differences are found for Mississippi Basin outflow. Much if not all of this error is likely due to the neglect of evaporation in the modern day precipitation climatology (Legates and Willmott, 1990) that is used by the GSM. However, it is also possible that the climatology is biased with excess precipitation. In future work, we will explore other precipitation climatology data-sets along with modifications to account for evaporation. For the work herein, however, we have chosen to scale precipitation over ice-free land by 1/1.34 for the NW sector and 0.3–0.5 for the eastern and southern sectors in order to approximately match present day outflows.

The drainage module is run at the same spatial resolution as the ISM. Consideration was given to running the drainage solver at a higher resolution. However, given the resolution of the rest of the glacial systems model (limited by computational resources) and the uncertainties in the ice-margin chronology, we decided that matching the resolution of the ISM along with hand-checking provided the most accurate and analysable solution. A significantly higher model resolution would also have precluded hand-control in the production of the base drainage topography.

A few key grid-cells of the drainage topography are given time-dependent values to account for sub-grid changes in surface elevation with margin recession. These time dependences were generally computed based on approximate interpolation between appropriate time-slices of the margin chronology across a much higher resolution version of the drainage topography. The key exception to this is the imposition of time-dependent changes to the elevation of the sill for the southern Lake Agassiz outlet to account for inferred erosion of the sill. For this case, the elevation of the sill is initially set to 332 m. Upon overflow after −14.4 ka, sill elevation is reduced to 325 m. Upon overflow after −13.6 ka, sill elevation is reduced to 300 m. And finally after −13.0 ka, sill elevation is reduced to 296 m upon overflow (and after −12.9 ka even if no overflow occurs).

Given the truncated model grid (which is cutoff at 35°N) along with poor constraints on precipitation chronologies and lack of accounting for evaporation, our analyses will focus on meltwater and ice calving (and for computational simplicity, precipitation over ice-covered ablation zones) as flux inputs in the drainage computation. As an upper bound, we will also provide some discharge chronologies that include scaled precipitation over ice-free land.

2.2. Climate and margin forcing

In order to capture uncertainties related to poorly constrained dynamical processes, our analyses are based on large ensembles of model runs, with 22 ensemble parameters that are varied between ensemble members. These ensemble parameters include the 20 parameters from Tarasov and Peltier (2004) along with two new parameters used to force Heinrich events 1 and 0 in the model. In the ensembles, these two forcings are imposed from −17.2 to −16.1 ka (extracted from the range of dates in Hemming, 2004) and from −12.0 to −11.4 ka, and take the form of an ad hoc ablation applied over Hudson Bay, Foxe Basin, and Hudson Strait. These forced Heinrich events were imposed to improve fits to the RSL data in the core region of the ice sheet. Aside from these two Heinrich event parameters, the till viscosity, and the three calving parameters, the remaining 16 ensemble parameters control variations in the climate forcing.

The time dependence of the climate forcing is largely controlled by a glacial index, $I(t)$, derived from the inferred temperature history for the Greenland summit region. Using the GRIP δ^{18}O record and the observed value for the δ^{18}O lapse rate in central Greenland of $\lambda_\delta = -6.2\,\mathrm{mil}^{-1}\,\mathrm{m}^{-1}$ (Johnsen et al., 1989), the glacial index is defined as follows:

$$I(t) = \frac{(\delta^{18}\mathrm{O}\ (t) - \delta^{18}\mathrm{O}\ (0) - \lambda_\delta * (h_{\mathrm{GRIP}}(t) - h_{\mathrm{GRIP}}(0)))}{(\delta^{18}\mathrm{O}\ (\mathrm{LGM}) - \delta^{18}\mathrm{O}\ (0) - \lambda_\delta * (h_{\mathrm{GRIP}}(\mathrm{LGM}) - h_{\mathrm{GRIP}}(0)))}, \quad (1)$$

with the surface elevation of the GRIP site ($h_{\mathrm{GRIP}}(t)$) taken from the tuned model (GrB) of Tarasov and Peltier (2003). This index weights the time-dependent linear interpolation between a present day observed climatology and LGM climate fields derived from a composite of the PMIP archived −21 ka general circulation model simulations (http://www-lsce.cea.fr/pmip/index.html) as detailed in Tarasov and Peltier (2004). The present day temperature climatology is derived from a 14 year mean (1982–1995) of re-analysed 2 m monthly mean temperature fields (Kalnay et al., 1996). The environmental lapse rate is interpolated between a high-latitude weighted modern value of 7.5 °C/km (based on the results of Rennick, 1977) and an LGM value of 6 °C/km using glacial index weighting. The lower LGM environmental lapse rate was chosen to conform to expected conditions along the summertime southern ice-sheet margin, which is the ice-sheet region most sensitive to the value of surface temperature.

Precipitation is exponentially interpolated between the present day observed climatology $P(0,x,y)$ (Legates and Willmott, 1990) and the LGM field from the PMIP ensemble $P(\mathrm{LGM},x,y)$ using the following expression:

$$P(t,x,y) = RP_{SM}(t,x,y)\cdot P(0,x,y) \times \left\{\frac{fP_W(t,x,y)\cdot fP\cdot P(\mathrm{LGM},x,y)}{P(0,x,y)}\right\}^{I(t)^{\Theta_P}}. \quad (2)$$

We introduce the "ensemble phase factor" (Θ_P) to parameterize some of the uncertainty associated with the transition from interglacial to glacial atmospheric states. fP is a global ensemble scale parameter. To improve fits

to geophysical observations in western and southwestern Canada, two additional ensemble scale parameters (RP_W and fP_SM) allow for regional enhancements during the −30 to −10.6 ka period. These enhancement factors can be partially justified as providing corrections to the results of the PMIP model runs, which were carried out with a surface topography that lacked a significant Keewatin ice dome. We hypothesize that this ice dome diverted the jet stream southward, and subsequent baroclinic instability along the southern margin would have enhanced regional precipitation. The necessity of the existence of the Keewatin Dome, originally inferred on the basis of surface geomorphological considerations by Dyke and Prest (1987), was recently demonstrated in Peltier (2002) and Tarasov and Peltier (2004) on the basis of absolute gravity and very long baseline interferometry (VLBI) observations.

To capture the inter-model variance of the PMIP runs, three empirical orthogonal basis functions (EOFs) for temperature and two for precipitation are also included in the ensemble parameter set. Furthermore, a strong regional topographic feedback on precipitation is provided via the desert-elevation effect (Budd and Smith, 1981) in which precipitation is reduced exponentially with height (above a cutoff elevation). Climatologically, this may be seen to be required to correct the GCM precipitation fields to the higher elevations of the high-resolution ISM grid. In order to fit RSL constraints, we have found it necessary, however, to impose much stronger desert-elevation regional cutoff factors than can be accounted for on the basis of the decrease in saturation vapour pressure with elevation. We justify this once more on the basis of our hypothesized atmospheric reorganization due to the presence of the large Keewatin dome. These regional cutoffs are imposed only during the −30 to −10.6 ka period when a significant Keewatin dome was found to be present in preliminary ensemble analyses.

Even with the relatively large number of ensemble parameters, the above parameterization of climate through the glacial cycle is much too limited to capture the complexities of glacial climate variation. During the deglacial period, climate will most significantly control margin position. The availability of a high-resolution deglacial digitized margin chronology (Dyke et al., 2003; Dyke, 2004) offers the opportunity of a strong reduction in the impact of climate forcing uncertainties on the model. To this end and as in Tarasov and Peltier (2004), we directly impose the inferred ^{14}C controlled margin chronology (using the INTCAL98 ^{14}C to calendar year conversion of Stuiver et al., 1998a) through modifications to the surface mass-balance. The −21.4 to −6.8 ka subset of the margin time-slice dates are shown in Table 1.

In order to capture margin chronology uncertainties and to increase dynamical consistency of the ice margin with the climate forcing and ice-sheet, Tarasov and Peltier (2004) employed a 100 km buffer zone around the digitized margin in which modifications to the surface mass-balance were not imposed. However, initial drainage results obtained using this approach did not deliver significant Mississippi meltwater flux during mwp1-a in disagreement with the paleo record. Correction of this problem required a redefined treatment of this buffer zone to enforce a closer fit of the modelled ice-sheet margin to the margin chronology. In detail, the margin field still retains a buffer zone represented by field values of 1 and 2 for grid-cells, respectively, outside and inside the digitized ice margin. Ice-margin field values outside the buffer zone are given values of 0 (ice free) and 3 (ice-covered). Margin field values are smoothly interpolated between margin chronology time-slices. In grid-cells that are ice-free, positive mass-balance is smoothly imposed starting at interpolated margin field values of 1.8 and becomes full strength for a margin field value of 2.5. Conversely, net ablation is smoothly imposed on ice-covered grid-cells below 1.8 and becomes full strength at a value of 0.8. Ensemble sensitivity to margin buffer width is examined below.

Table 1
−21.4 to −6.8 ka sequential subset of margin chronology

Timeslices: *calendar ka* (^{14}C ka)				
−21.4 (18)	−20.8 (17.5)	−20.2 (17)	−19.65 (16.5)	−19.1 (16)
−18.5 (15.5)	−17.9 (15)	−17.35 (14.5)	−16.8 (14)	−16.2 (13.5)
−15.6 (13)	−14.7 (12.5)	−14.1 (12)	−13.45 (11.5)	−13.0 (11)
−12.7 (10.5)	−12.0 (10.25)	−11.45 (10)	−11.0 (9.6)	−10.75 (9.5)
−10.2 (9)	−9.5 (8.5)	−9.0 (8)	−8.6 (7.8)	−8.45 (7.7)
−8.4 (7.6)	−8.0 (7.2)	−7.8 (7)	−7.45 (6.5)	−6.8 (6)

Margin forcing is also smoothly introduced beginning at 1.5 ka prior to the first time-slice (−21.4 ka) of the digital chronology. Given that the geological evidence indicates that most regions of the ice sheet reached full margin extent by about 4 ka prior to the conventional date of LGM of 21 ka (Dyke et al., 2002), our 1.5 ka onset period is, if anything, overly short. A short onset period was chosen so as to allow investigation of the maximum extent to which isostatic disequilibrium at LGM might "contaminate" the geophysical inversion of RSL data.

Initial ensemble analyses led to the conclusion that full margin forcing was too restrictive with respect to obtaining acceptable fits to certain RSL observations. These were generally sites, where good fits could be obtained if grounded ice in adjacent marine channels were replaced by ice-shelves or open water. Given that glaciological observations provide only weak constraints on past marine margin locations and that they are especially hard pressed to distinguish between ice-shelves and grounded ice, we therefore allow ice calving to over-ride the margin chronology (which obviously only occurs in the marine sectors of the ice sheet).

2.3. Calibration, ensemble scoring, and geophysical data

The ensemble results presented in this paper originate from an ongoing Bayesian calibration of the GSM against a large set of RSL and geophysical observations (Tarasov

Table 2
GSM input and constraint data summary, detailed in text

Component	Data source	Main direct impact
Present day precipitation	Observed climatology (Legates and Willmott, 1990)	
Present day temperature	Reanalysis data-set (Kalnay et al., 1996)	
LGM precipitation	PMIP ensemble	Ice geometry
LGM temperature	PMIP ensemble	Ice geometry and pre-LGM margin location
Climate interpolation	GRIP δ^{18}O (Johnsen et al., 1989)	Ice geometry and meltwater flux
Sediment map for till deformation	Derived from sediment map (Laske and Masters, 1997) and surficial geology map (Fulton, 1995)	Ice geometry
Deep geothermal heat flux	Map of Pollack et al. (1993)	Ice geometry and basal melt
Earth radial viscosity	VM2 (Peltier, 1996; Peltier and Jiang, 1996)	Ice geometry and surface drainage routing
Earth radial elasticity	PREM model (Dziewonski and Anderson, 1981)	
Eustatic sea-level chronology	SPECMAP δ^{18}O chronology (Imbrie et al., 1984)	Marine ice-margin and coastal inundation
Deglacial margin chronology	(Dyke et al., 2003; Dyke, 2004)	Deglacial ice-margin location and surface drainage
RSL data	University of Toronto RSL database	Model calibration → ice geometry
$\dot{R}$ (Yellowknife)	(D. F. Argus, pers. comm., 2004)	Deglacial Keewatin dome ice thickness
$\dot{g}$ transect	(Lambert et al., 2001)	South central deglacial ice thickness
Present day drainage topography	MDhby derived from HYDRO1K DEM	Surface drainage determination
Upper Campbell SO strandline	(T. G.Fisher, pers. comm.)	Regional ice thickness → drainage routing
Wampum strandline	(Teller et al., 2000)	Regional ice thickness → drainage routing
NW strandlines	see Table 5	Regional ice thickness → meltwater flux

et al., manuscript in preparation). The calibration procedure uses a set of multilayer perceptron neural network simulators of the GSM to extensively sample the model phase space. The posterior distribution for GSM parameter vectors given the constraint data are proportional to the product of the prior probability distribution of the parameters and the probability of fitting the constraint data given the parameters. Markov Chain Monte Carlo sampling from this posterior distribution (using the neural network simulators) provides new trial parameter vectors for input into the full GSM. Results from the full GSM with the new parameter vectors are then employed to further train the neural networks for further iterative calibration. The largest uncertainties that cannot be accounted for in the calibration procedure are the limited phase space of the GSM along with uncertainties in the applied margin chronology (Dyke et al., 2003; Dyke, 2004) and the limited spatio-temporal coverage of the constraint data-set (as discussed below).

Given the large parameter space of our ensemble model set-up and the severe parameter modifications that are imposed on replicated sensitivity ensembles, ensemble runs are first sieved by a set of primary constraints. Firstly, we assume that Hudson Bay must have a minimum ice thickness of 400 m at −25 ka to provide for a minimal possibility of adequate ice supply for Heinrich event 2 at −24 ka. Secondly, we require the computed value of vertical motion ($\dot{R}$) at Yellowknife to be within two standard deviations of that observed. Finally, initial calibrations tended to develop "ice holes" in central Quebec leading up to LGM, likely due to difficulties in fitting the southeast Hudson Bay RSL data. Physically, it is unlikely that ice would grow from the southern margin of Quebec towards its centre. As such, runs with significant central Quebec low spots in the LGM ice configuration are also sieved from the ensemble.

Runs that passed these primary constraints were then scored with respect to fits to high-quality RSL observations from 24 geographically dispersed and data-rich sites. RSL data are only available for regions that were previously inundated by the sea and are now exposed land. As such, most of the western region of the Laurentide ice sheet lacks any RSL constraint. This is especially problematic with respect to drainage routing as Lake Agassiz outlets are all far from RSL data sites. Fortunately recent geodetic observations for this region provide additional constraints. Revised results from VLBI provide a measurement of the present day rate of vertical motion of 6.5 ± 1.5 mm/yr at Yellowknife (Argus, pers. comm., 2004). Furthermore, a recently completed 6 point transect of repeated absolute gravity measurements (Lambert et al., 2001) has provided measurements of the time derivative of the surface gravitational acceleration ($\dot{g}$) for the south central region of the Laurentide Ice Sheet running from Churchill Manitoba to Iowa City, Iowa. Model fits to these observations are therefore also included in the ensemble scoring. Further details are provided in Peltier (2002, 2004) and Tarasov and Peltier (2004).

A summary of the input and constraint data for the GSM is provided in Table 2. When considering the "main direct impacts" in the table, one should also keep in mind that changes to ice geometry will affect meltwater fluxes and possibly surface drainage routing.

3. Results and analyses

We have extracted a selection of 30 "best runs" from an on-going Bayesian calibration of modelled Laurentide

deglaciation. It should be noted that this ongoing calibration is subjected to a much larger RSL dataset than that used for scoring the drainage results in this paper. To help ensure that our base ensemble was not locked into a local minimum in the calibration space, we chose a number of "best" fits using a varied set of weightings for RSL fit, margin fit just prior to onset of margin forcing, and fits to geodetic constraints.

As will be detailed below, after initial investigations with our base ensemble set ("13A"), significant mis-fits were found with respect to key strandlines for glacial lakes McConnell and Agassiz. Regional precipitation forcing (including desert-elevation effect) adjustments and a modification to the margin forcing were then applied to reduce the inferred mis-matches for Lake Agassiz strandlines (and to a lesser extent those of lake McConnell). As these modifications were applied in regions relatively far from RSL data, these applied adjustments had limited impact on the overall fit to RSL data. One of the resultant best-fit ensembles ("13Z") was further subject to a number of margin and climate forcing variations in order to bracket key results. Results from three of these variant ensembles (13G, 13R, 13S) are also presented. As well, two other ensembles, 13P and 13C, with, respectively, strong lower bound and weak upper bound sized Keewatin Domes were also created. The various ensembles are summarized in Table 3.

In the course of this project, it became clear that there are significant ensemble sensitivities to the width of the margin forcing buffer region. Our initial ensembles used a ± 100 km wide buffer region on a high-resolution grid that was subsequently discretized to the 0.5° latitude by 1.0° longitude resolution of the model. The width was so chosen to account for the combination of the ± 50 km uncertainty of the margin position chronology for each time slice, sub-time-slice margin oscillations, and marginal ablation zones. However, this buffer zone tended to produce wide (multi-grid-cell) thin ice regions along certain segments of the ice margin. These thin ice sections represent regions where the ISM is unable to dynamically fit the margin chronology suggesting limitations with some combination of the model, climate forcing, and/or the margin chronology. The strandline tuned ensemble 13G uses the ± 100 km wide buffer region. However, to stay true to the assumed margin chronology, the base ensemble 13Z was tuned with an ± 80 km buffer zone, which tended to produce a single grid-cell wide buffer zone on each side of the southern ice margin in the model.

Another issue of possible significance with respect to deglacial drainage and it's impact on NADW formation is the exact timing and ice dynamical source of the H0 event. Heinrich event 0 is generally much less distinctive in oceanic sedimentary cores than H1 (e.g., Kirby, 1998). An exception to this is the carbonate record from the Orphan Knoll core HU91-045-094-P (Stoner et al., 1996), downstream of Hudson Strait, which displays a strong H0 pulse. Furthermore, this pulse starts just after the Vedde Ash layer (Hillaire-Marcel, pers. comm., 2004), which has a well constrained date of -12.0 ka in the GRIP and GISPII ice cores. This largely rules out the possibility that Hudson Strait ice discharge during H0 was the dynamical trigger for the reduction (or cessation) of NADW formation during YD onset. The more limited spatial extent of H0 signatures also suggests that the extent of Hudson Bay ice drawdown was less than that of H1, though warmer sea surface temperatures and altered ocean currents may also have limited the extent of ice-rafting. To account for this uncertainty, we have explored different H0 representations in the model. However, all variants tested had no significant impact on non-Hudson Strait drainage and are therefore not presented herein. It should be noted, that in order to fit the RSL data for the Hudson Bay and Foxe

Table 3
Ensemble comparison

Ensemble	Description	Margin buf. width (km)	$\dot{R}$ error (mm/yr)	Max h_W (m)	mwp1-a m eustatic
13A	Base, no strandline tuning	100	0.00	3247	9.9 ± 0.3
13G	Base, strandline tuned	100	0.30	3523	9.4 ± 0.3
13P	Strandline tuned, reduced NW precip.	80	-1.41	2557	7.8 ± 0.2
13Z	Base, strandline tuned	80	0.27	3539	8.7 ± 0.4
13R	GISPII climate chronology	80	0.47	3482	6.0 ± 0.3
13S	$dt/2$ margin forcing delay	80	0.56	3522	8.0 ± 0.3
13C	High volume variant of 13Z	100	0.30	3562	9.6 ± 0.3

Mean $\dot{R}$ value is for Yellowknife. The observed 1 sigma range is ± 1.55 mm/yr. h_W is the maximum Keewatin dome elevation. mwp1-a contributions are for -14.6 to -14.0 ka interval (except for ensemble 13R which uses -14.7 to -14.2 ka). Ensemble 13Z is the base ensemble with approximate strandline tuning. Ensembles 13C, 13P, 13R, and 13S are variants of 13Z. 13C imposes a wider region (115°W to 100°W and 54°N to 66°N) of enhanced precipitation over the NW along with a 100 km margin buffer. This allows NW routing of Lake Agassiz outflow during the early YD but also weakened Lake Agassiz strandline fits. 13P imposes a stronger desert elevation effect over the NW and has the best fits to Lake Agassiz strandline data. 13R uses the GISPII δ^{18}O chronology for the climate forcing instead of the default GRIP δ^{18}O chronology. 13S delays the margin forcing chronology (a subset of which is listed in Table 1) by a half time-step towards the subsequent time-slice. 13G is another base variant that uses a 100 km margin buffer and is also tuned to the Lake Agassiz strandlines.

Basin regions, the time-average ice thickness after H1 must be reduced by some form of forced ice drawdown process in the model.

In what follows, we will first discuss computed regional drainage chronologies. In order to enable a first order validation of the results, we then examine proglacial lake level, area, and volume chronologies. The robustness of the Lake Agassiz outflow routing history is subsequently analysed. Finally, climatic consequences of the new drainage history are considered.

3.1. Regional drainage chronologies

Ensemble means and 1 sigma confidence intervals were computed by weighting the contributions of individual runs of the model according to a metric based upon the goodness of fit of predictions to RSL and geodetic data and of predicted ice-margin location just prior to the imposition of the independent margin chronology. As such, the confidence intervals do not include uncertainties associated with the imposed margin chronology nor with the limited ensemble coverage of the possible deglacial phase space. Pacific discharge (Fig. 3a) begins to decrease immediately after LGM, interrupted only by relatively substantial pulses coincident with mwp1-a (−14.4 ka) and during the YD. All four ensembles for which results are shown have a significant pulse at −12.3 ka, while 13Z and its two variants also have a weaker pulse at −12.5 ka. Either of the YD pulses would be consistent with a 10.5 ^{14}C ka (reservoir corrected) date for a massive outburst flood through the Fraser Lowlands inferred on the basis of anomalous clay horizons in ODP cores collected from Saanich Inlet, Vancouver Island (Blais-Stevens et al., 2003) if one uses the CALIB4.1 (Stuiver et al., 1998b) conversion for this date of −12.5 ka (with −12.8 and −11.8 ka 1 sigma bounds). The converted date of −11.0 ka obtained by Blais-Stevens et al. (2003) appears to be erroneous and possibly due to the use of an outdated ^{14}C calibration.

Early Pacific discharge is largely due to coastal calving. Significant Cordilleran margin recession does not occur until after −16.8 ka (14.0 ^{14}C ka) which is reflected in the discharge chronology with a small pulse at −16.5 ka. It is also clear from Fig. 3a that aside from the −12.5 ka (and −12.3 ka for 13Z) pulse, the only substantial impact of hydrological tuning was to increase early deglacial discharge for ensemble 13P. As topographic relief provides strong drainage basin boundaries, Pacific drainage discharge uncertainties are largely related to surface mass-balance, with only minor sensitivity to drainage basin boundary and routing issues.

The main impact of the inclusion of precipitation over ice-free land (13Zp in Fig. 3a) is the removal of the downward baseline trend in the computed Pacific discharge. Given the strong topographic relief imposed by the Rocky Mountains, there is little change in overall area of the Pacific drainage basin.

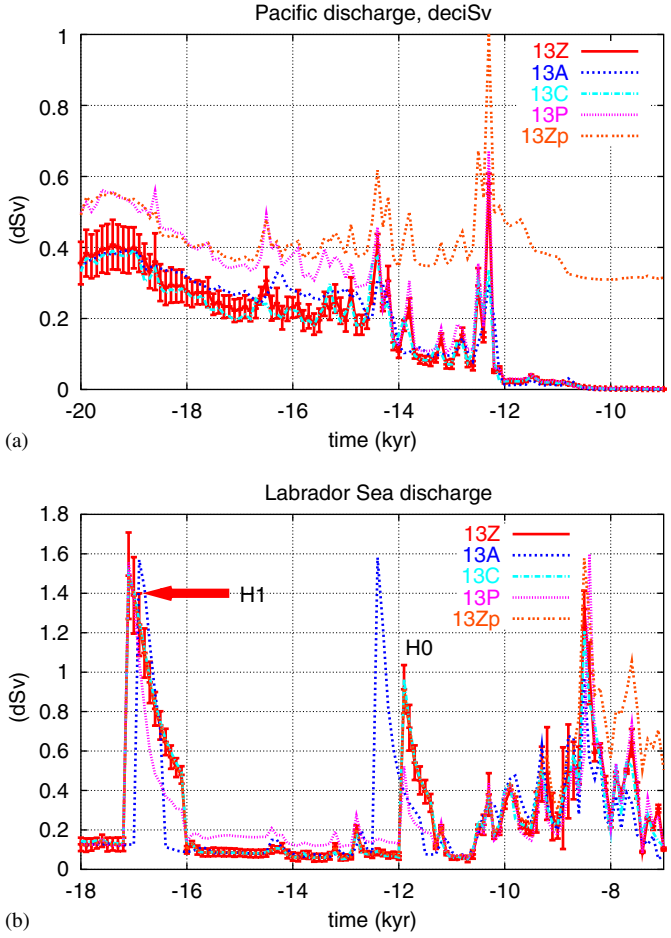

Fig. 3. Computed Pacific "(a)" and Labrador Sea "(b)" meltwater and iceberg discharge with 1 sigma confidence intervals for ensembles 13Z, 13A, 13C and 13P. 13Zp is ensemble 13Z with precipitation over ice-free land included assuming 50% evaporation. Other ensemble differences are summarized in Table 3. The confidence intervals are determined by fit to constraint data. They do not include uncertainties associated with the margin chronology nor with limited coverage of the glacial phase space by the GSM.

Discharge into the Labrador Sea region (Fig. 3b, southeast Ellesmere Island to Newfoundland) is dominated by large forced-calving events corresponding to Heinrich events 1 and 0 and a −8.5 ka pulse that occurs for all hydrologically tuned ensembles during the collapse of the Hudson Bay dome. The difference in H1 and H0 between the ensemble 13A and the other ensembles shown in Fig. 3b is purely the result of the various imposed Heinrich event forcings. The magnitude and duration of the forced Heinrich events are poorly constrained. However the 1.5 dSv peak and the 1.0 dSv mean Labrador Sea discharge (over the first 500 years of the forced H1 event) of ensemble 13Z are below the 1.5–3.0 dSv over 500 year estimate of Hemming (2004) for a typical Heinrich event. Moreover, the Markov Chain Monte Carlo sampling that we are employing in the ensemble calibration tends to pick out the strongest Heinrich event forcing parameters allowed by the model parameterization. This arises because the regional

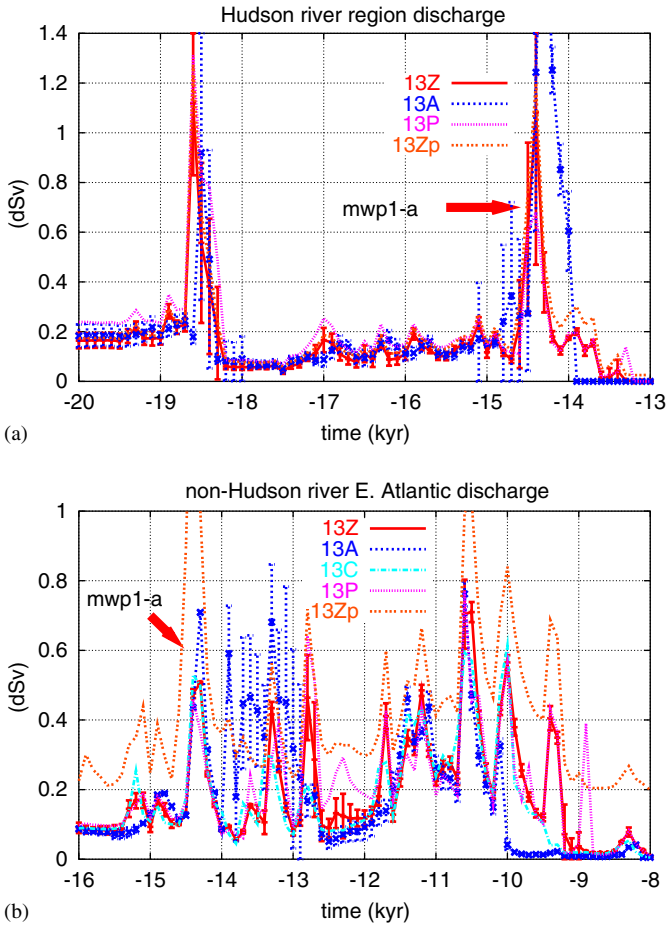

Fig. 4. Computed Atlantic discharge as per Fig. 3. Non-Hudson River discharge is all Atlantic discharge north of the Hudson River and south of Newfoundland and is dominated by discharge into the Gulf of St. Lawrence (with minor remaining contributions from Nova-Scotia and the Bay of Fundy region).

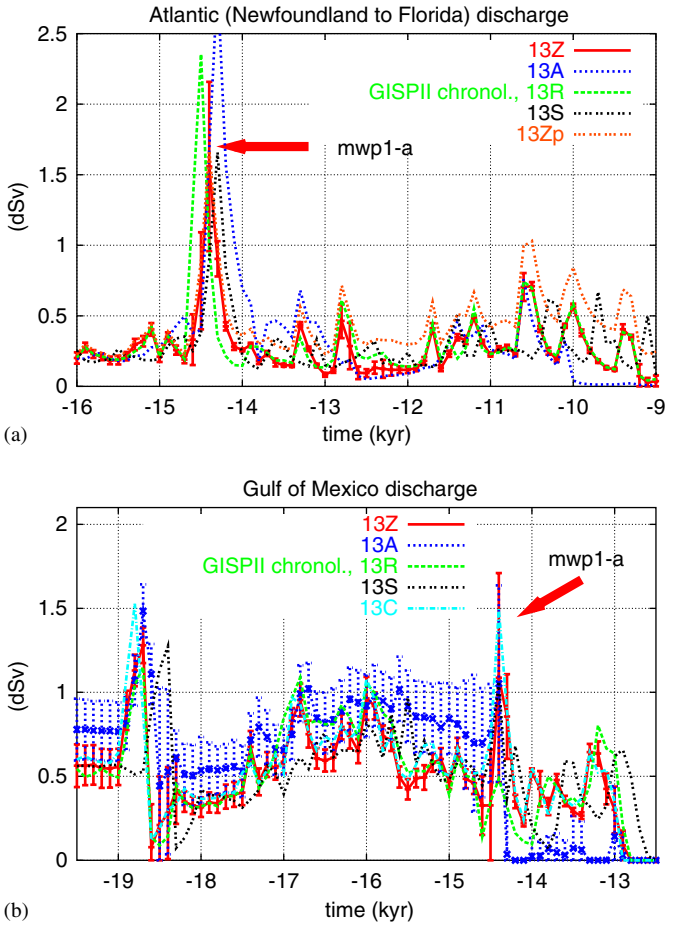

Fig. 5. Sensitivity of computed meltwater discharge to modified ensembles for Atlantic Ocean "(a)" and Gulf of Mexico "(b)". The ensembles are described in Table 3.

RSL data appear to require a relatively small time-averaged thickness of ice over Hudson Bay, and massive calving events are the only dynamical means to achieve this until termination of the YD when regional warming allows significant coastal ice ablation. After −10.6 ka, discharge oscillations are largely controlled by the margin chronology.

Atlantic discharge (Newfoundland to Florida) is dominated by two outlets, the Gulf of St. Lawrence and Hudson River (Figs. 1 and 4). Hudson River discharge is concentrated in two large peaks at −18.6 ka and during mwp1-a at −14.4 ka (Fig. 4a). Both peaks arise from margin recessions in the margin chronology that allow opening of an eastward choke-point just east of Lake Erie ("EC" in Fig. 6a). The first peak corresponds to a temporary eastern diversion of south central meltwater outflow from the Mississippi drainage basin (Fig. 5b). During the mwp1-a peak, some ensemble runs only have Great Lakes Basin outflow diverted to the Hudson River (Fig. 6b), while others have eastern diversion of south central meltwater outflow as well. This results in ensemble discharge peaks for both Atlantic and Gulf of Mexico outlets. Discernible meltwater discharge into the Hudson River ceases after −13.3 ka.

The Gulf of St. Lawrence discharge (dominant component of non-Hudson River Eastern Atlantic discharge) remains below 0.15 dSv until −15.5 ka (Fig. 4b). Even though the Great Lakes basin outflow is through the Hudson River during mwp1-a and until about −13.7 ka, substantial discharge occurs into the Gulf of St. Lawrence and Bay of Fundy during mwp1-a. Gulf of St. Lawrence (meltwater and iceberg only) discharge at all times and for all ensembles is below 0.9 dSv.

Some validation of the Gulf of St. Lawrence discharge chronology can be found in reconstructed sea-surface salinity chronologies derived from dinoflagellate-cyst assemblages in three marine sedimentary cores from Cabot Strait, the Laurentian channel and NW North Atlantic (de Vernal et al., 1996). The −13.3 to −13.1 ka onset of significant post mwp1-a St. Lawrence outflow is approximately coincident with the reconstructed pre-YD sea-surface salinity minimum for the Cabot Strait Gulf of St. Lawrence outlet. The only reconstructed sea-surface salinity decrease that is common to the three sedimentary

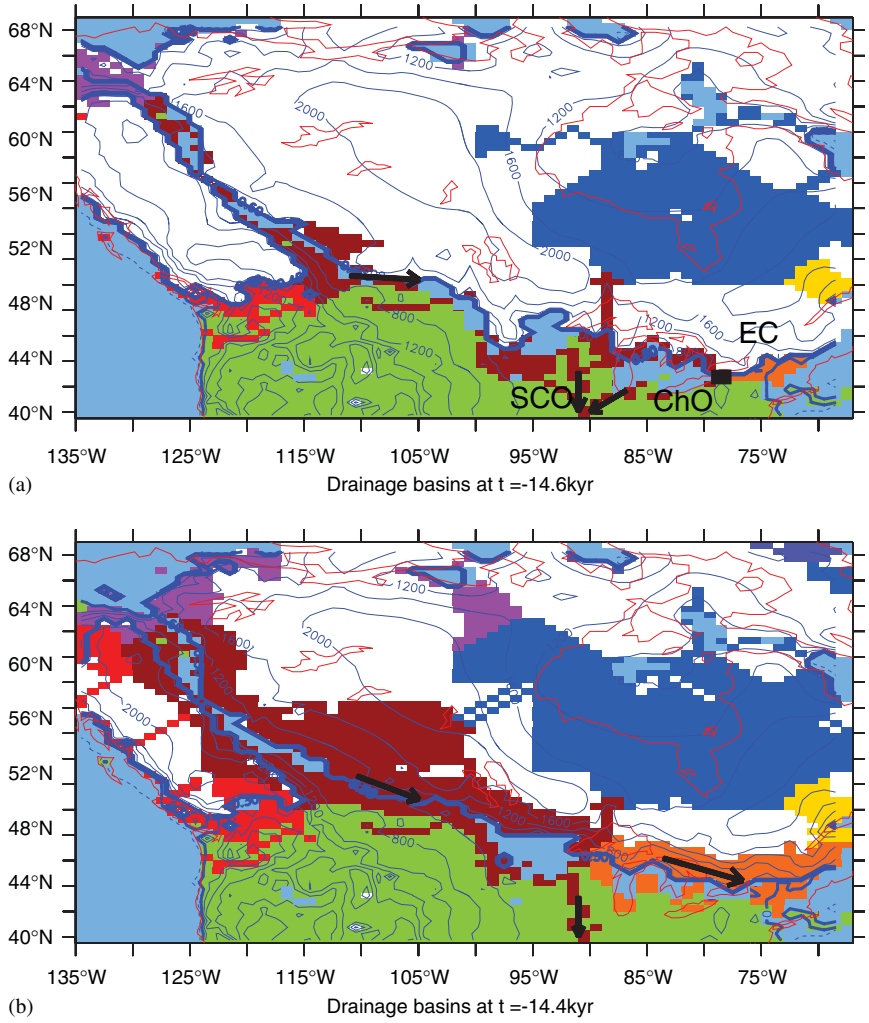

Fig. 6. Drainage basins at −14.6 ka "(a)" and −14.4 ka "(b)" for best-fit run nn1082. The colour code for the drainage basins is as follows: red: Pacific, purple: NW, dark blue: Labrador Sea, yellow: Gulf of St. Lawrence, orange: Hudson River, brown: Mississippi. These drainage colours are applied only to grid-cells that are either contributing or routing meltwater (or iceberg discharge) and are not filled by lakes. The large expanses of meltwater that are far interior of the ice margins are generally due to basal meltwater generation. Proglacial lakes are shown for grid-cells filled to at least the mean sub-grid elevation of the cell. Arrows indicate drainage basin outflow. White regions are ice-covered and meltwater free. The ice margin is shown in blue. Also shown is the location of the early eastern (EC) choke-point. Outflow from the St Croix (SCO) and Chicago (ChO) outlets are also indicated.

cores is bracketed by 10.2 and 10.1 ^{14}C ka dates and might correspond to one or all of the 0.4–0.5 dSv St. Lawrence outflow spikes that occur between −11.7 and −11.2 ka. It is also possible that the date is too old due to carbonate contamination and that the salinity spike actually corresponds to the subsequent largest discharge peak at −10.6 ka. The lack of significant Champlain Sea freshening until after −10.5 ^{14}C ka inferred by Rodrigues and Vilks (1994) along with the high YD (most clearly during onset and termination) sea-surface salinities reconstructed for the Gulf of St. Lawrence region by de Vernal et al. (1996) arguably contradict the significant −12.8 ka discharge peak for ensembles 13Z and 13P shown in Fig. 4b. This suggests that the eastern −12.8 ka routing of Lake Agassiz outflow in these two ensembles (discussed below) appears to be invalidated by the observations.

With regards to possible impacts of meltwater discharge on the Atlantic MOC, of much more interest is the total Atlantic (Hudson River and Gulf of St. Lawrence basin) discharge. The ensemble Atlantic discharge is relatively robust as is evident in the general agreement across most ensemble variants shown in Fig. 5a. Much of the drainage basin for this region is well populated by RSL data, and therefore is highly constrained overall in the ensemble. Atlantic discharge is however sensitive to uncertainties associated with the margin chronology as represented by ensemble 13S. This ensemble is a replicate of 13Z with margin forcing (and topographic time dependence in the drainage solver) delayed by one half of the interval to the next time slice in the margin chronology (a subset of which is listed in Table 1). For instance, the −16.2 ka time-slice becomes the −15.9 ka time-slice. As such, it represents an arguably extremal phase shift of the margin chronology. While 13S produces only a 100 year phase shift on the timing of mwp1-a, it has much stronger impacts during the onset of the YD and after −10.7 ka. Uncertainties

associated with the climate forcing chronology as represented by ensemble 13R are also about 100 years for the timing of mwp1-a. The only other significant uncertainty is that associated with the magnitude of the mwp1-a contribution. The peak (100 year mean) contribution across all ensembles ranges to 2.9 dSv. Ensemble 13Z has the lowest peak contribution of 1.5 ± 0.6 dSv. The 100 year phase shifts in the timing of mwp1-a in response to changes in climate (13R) or margin (13S) forcing chronologies suggest that the timing of the event is relatively robust.

The lack of RSL constraints for the south central region of the ice sheet and the weakness of the geodetic constraints for this region manifests as large error bars for Gulf of Mexico discharge estimate for ensemble 13A (Fig. 5b). However, the strandline tuned ensemble 13Z has much narrower error bars, partly on account of it being a lower mass-flux bound version of 13A. This is apparent in that for much of the deglacial history, the 13Z and 13C ensemble discharge approximately follows the 1 sigma lower bound values of 13A.

Our reconstructed Mississippi outflow (Gulf of Mexico discharge, Fig. 5b) is in approximate accord with the first two of the 13.4 ^{14}C ka (approximately −16.3 to −15.7 ka 1 sigma range), 12.6 ^{14}C ka (approximately −15.4 to −14.2 ka 1 sigma range), and 11.9 ^{14}C ka (approximately −14.1 to −13.5 ka 1 sigma range) mega floods inferred on the basis of new δ^{18}O and carbon isotope records (Aharon, 2003), though detailed comparisons are difficult given dating uncertainties with respect to reservoir effects and ^{14}C plateaus. ^{14}C dated records of reworked nanofossils suggest a trimodal history of Mississippi deglacial megafloods between 15.1 ^{14}C ka (approximately −18.4 to −17.6 ka 1 sigma range) and 12.2 ^{14}C ka (approximately −14.3 to −13.7 ka 1 sigma range) (Marchitto and Wei, 1995), which again may or may not correspond to the largest discharge peaks in Fig. 5b. The only Mississippi meltwater pulse that is clearly indicated across proxies is that during mwp1-a (Brown and Kennett, 1998). The one sigma upper bound discharge for all ensemble variants aside from 13R has its largest post −18.5 ka value during mwp1-a providing some concordance with the observations. The lack of substantial mwp1-a Mississippi discharge for this latter ensemble that uses the GISPII climate forcing chronology (13R) effectively rules out this chronological modification for at least this period. The large intra-ensemble scatter at −14.4 ka is due to switching between southern and eastern drainage outlets of Lake Agassiz shown in Fig. 6. It is also unclear whether the large discharge pulse that occurs around −18.7 ka is invalidated by the limited observations.

Examination of the drainage basins for one of our best-fit models shown in Fig. 6 offers more insight into the regional sourcing of meltwater during the mwp1-a interval. Initially, at −14.6 ka, the Mississippi is capturing almost all meltwater from southwest of Great Bear Lake in Nunavit to the eastern margin of Lake Erie. Outflow from the Great Lakes basin is via the Chicago outlet on the southwest corner of the Lake Michigan basin (“ChO” in Fig. 6) while Lake Agassiz region outflow is via the St. Croix to upper Mississippi river basin (“SCO” in Fig. 6). However, total discharge into the Mississippi is relatively small (Fig. 5b). At −14.5 ka and even more strongly at −14.4 ka, the loss of Great Lakes outflow into the Mississippi is compensated by the large meltwater flux from NW margin recession between the Cordilleran and Laurentide ice sheets (Fig. 6b).

A complete shutdown of southern discharge to the Mississippi basin occurs after −12.9 ka (−13.0 ka for ensembles 13A and 13C) as shown in Fig. 5b. This is robust for all runs using the base margin chronology. The ensemble variant 13S that delayed the margin chronology by half the time to the next time-slice extends southern discharge to −12.6 ka (using the SO spillway). However, given that ^{14}C dated material from sediment cores in the SO spillway indicate that it was inactive during the −12.82 to −12.62 ka interval (minimal 1 sigma time range, Fisher, 2003), it appears that the margin forcing chronological distortion of 13S is excessive for this time period (with the caveat that dated samples could have been reworked). Furthermore, not even one run passing primary ensemble constraints produced southern discharge after −12.6 ka. Such a permanent shutdown is also suggested by the δ^{18}O and reworked nanofossil records from Orca Basin (Marchitto and Wei, 1995).

Except for a 0.7 dSv pulse for ensembles 13Z and 13C during the mwp1-a interval, mean discharge into the Arctic Ocean (Fig. 7a) is generally below 0.4 dSv until the start of the YD. Confidence intervals for the largest peaks and response to ensemble variants are generally narrower than that for the Gulf of Mexico. The most significant characteristic consists of the very strong pulse at −12.8 ka (Fig. 7a). The meltwater and iceberg component of this pulse has a weighted value of 1.2 ± 0.2 dSv for ensemble 13Z, 1.3 ± 0.2 dSv for ensemble 13G, 1.4 ± 0.2 dSv for ensemble 13C, and a value of 1.8 dSv for one of the best RSL fit runs nn1305. When including the more poorly constrained contribution of precipitation over ice-free land, the total weighted discharge is now 1.6 ± 0.3 dSv for 13Z and 2.2 ± 0.2 dSv for 13C. Furthermore, the relative contribution of ice-free precipitation increases during the YD and thereby sustains a high level of total Arctic Ocean discharge throughout the YD (Fig. 7a). The significant contribution from precipitation over ice-free land is a result of two factors. First, the area of the Mackenzie drainage basin has been expanded due to the strong isostatic depression of the receding Keewatin ice dome. Second, regional late glacial precipitation has been enhanced by the Bayesian calibration procedure in order to fit the observed present day rate of uplift at Yellowknife. We hypothesize that this precipitation enhancement is justified on the basis of the orographic impact of the large ice dome upon the prevailing westerly atmospheric flow. Future GCM based analyses will test this hypothesis.

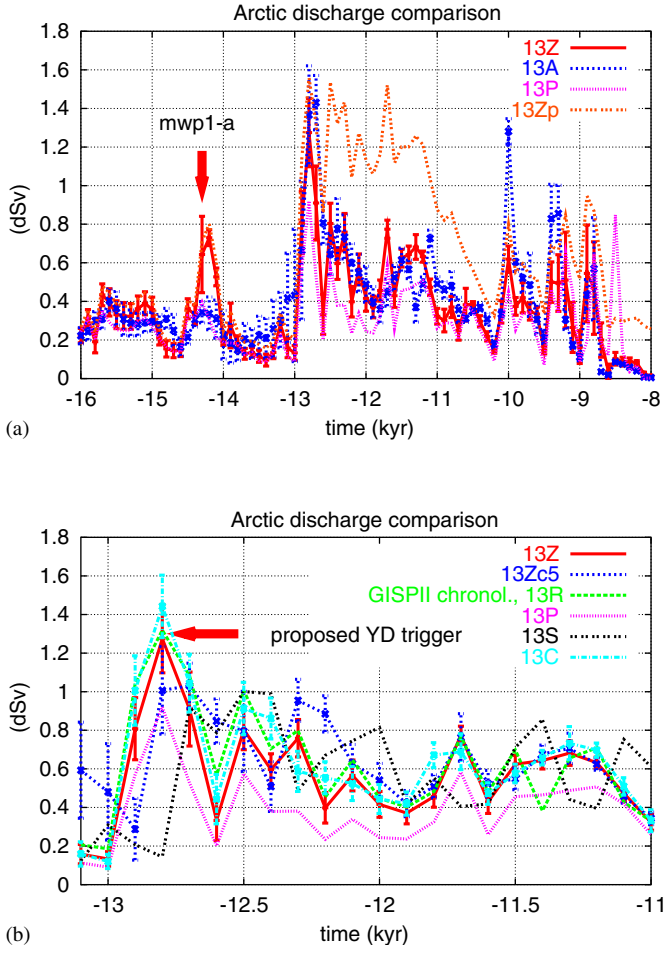

Fig. 7. Sensitivity of computed meltwater discharge to modified ensembles for discharge into the Arctic Ocean. One sigma confidence intervals are shown only for base ensemble. The ensembles are described in Table 3 with the addition of 13Zc5, which is a repeat of ensemble 13Z using the new IntCal04 ^{14}C calibration (Reimer et al., 2004) for the margin chronology.

Even the 13P ensemble variant with strongly reduced Keewatin precipitation produces a 0.9 ± 0.1 dSv pulse (1.0 ± 0.1 dSv including precipitation over ice-free land) at -12.8 ka (Fig. 7b). This ensemble variant produced weighted mean $\dot{R}$ values for Yellowknife that are at the lower 1 sigma confidence bound from geodetic observations (Table 3). Furthermore, the mean LGM ice volume of this ensemble is equivalent to 59 m of eustatic sea level, which is below what is required to fit the inferred global LGM eustatic sea-level drop given constraints on other LGM ice sheets. As such, this ensemble arguably represents an extreme lower limit for discharge into the Arctic Ocean.

The timing of the -12.8 ka NW pulse is also fully controlled by the margin forcing chronology. Only the 13S ensemble with delayed margin forcing is able to shift the timing of this pulse. And, as discussed above, ensemble 13S is in disagreement with observations for this interval due to its southern drainage of Lake Agassiz during the early YD. Just before submission of this work, version 5.0 of the Calib ^{14}C calibration program (Stuiver and Reimer, 1993) became available, which uses the new IntCal04 ^{14}C calibration (Reimer et al., 2004). As a test of model sensitivity to the ^{14}C calibration employed, ensemble 13Z was rerun with the new calibration. Significant changes in meltwater discharge timing involved a maximum of a 100 year phase displacement, and as such are well within the uncertainties of the margin chronology. The strongest impact was on Arctic discharge ("13Zc5" in Fig. 7b). But even for this case, the only significant differences were the sharp reduction in discharge at -12.9 ka and a more sustained discharge through the mid YD interval.

Overall, our computed regional meltwater discharge chronologies are generally robust across ensemble variants (aside from the chronologically modified 13R and 13S ensembles) and with relatively narrow confidence intervals. The key exception to this is the magnitude of regional contributions to mwp1-a. Margin and climate forcing chronology uncertainties, as parameterized in the ensemble variants 13R and 13S, are of order 100 years for mwp1-a. It should also be underlined that in addition to the above described uncertainties in the drainage modelling, there are further uncertainties associated with the model grid resolution, the visco-elastic representation of isostatic adjustment, the limited dimension of the parameter space for ensemble calibration and the geographically sparse coverage of the constraint data-set over western Canada. Given these uncertainties, we now turn to lake-level data for independent validation and strandline tuning of the deglacial meltwater drainage chronologies.

3.2. Lake levels

The margin recession of the Laurentide and Cordilleran Ice Sheets along with the isostatic depression of marginal regions allowed the formation of large proglacial lakes as illustrated in Figs. 8 and 9. The lake-level histories of these lakes are closely tied to the abrupt and large-scale changes in the configuration of regional drainage basins. Changes in lake level and thereby extent had significant impacts on shorelines, which potentially offer independent data for drainage history calibration and validation.

The inclusion of meltwater storage in the drainage solver allows numerous opportunities for comparison with paleo-hydrological proxy data. The most abundant proglacial lake proxies consist of strandlines, i.e. raised beaches and wave-cut cliffs from past inundation events. From the perspective of modelling, regional strandline elevations can be computed by adding contemporaneous grid-cell water depth (with an upper bound determined by maximum sub-grid relief) to the present day surface elevation of the high-resolution drainage topography. As a first example of this, we have computed a maximum strandline elevation chronology for Lake Agassiz that is presented in Fig. 10. Also shown in this figure are the chronologies of a number of synthetic proxies for Agassiz lake level. Geographic variations in isostatic rebound along with the constraint of maximum topographic relief (upon which paleo lakes can

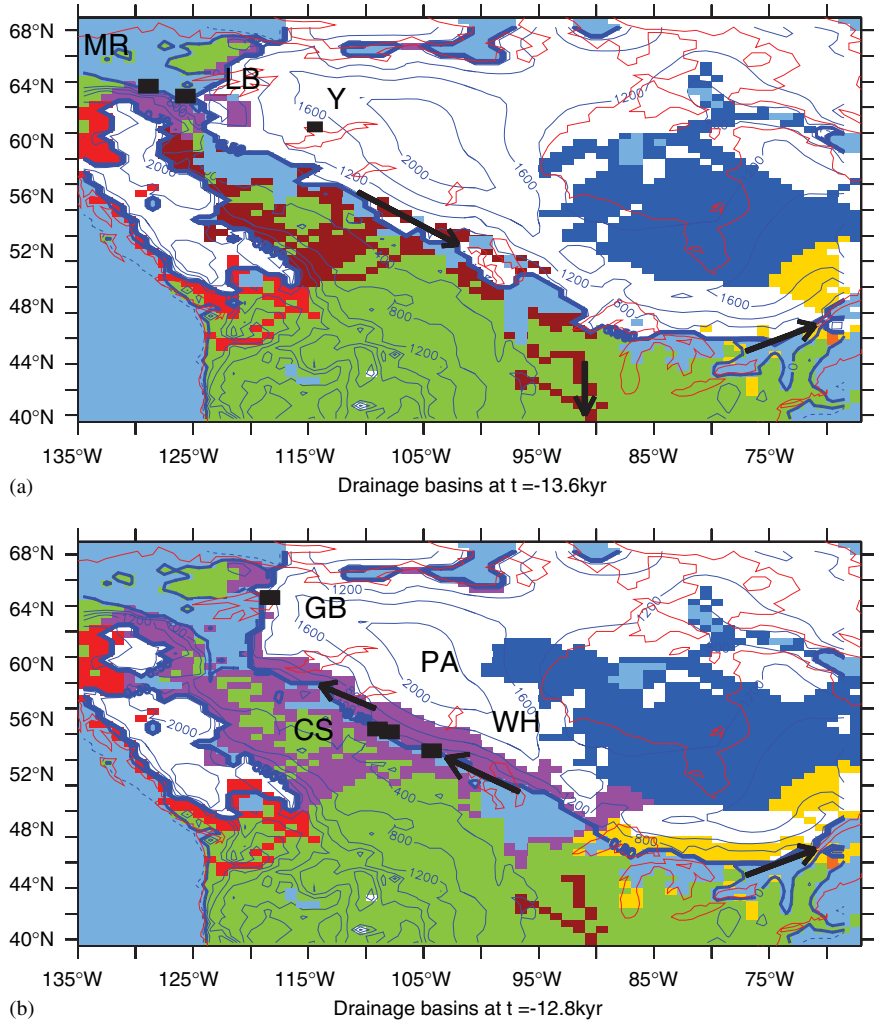

Fig. 8. Drainage basins at −13 ka "(a)" and −12.8 ka "(b)" for good fit run n1062. Drainage basin colour coding as for Fig. 6. Also shown are the locations of the Mountain River (MR) and Little Bear (LB) deltas discussed below along with the location of Yellowknife (Y) and the Great Bear (GB) and Patuanak (PA) strandlines. The Wapawekka Hills (WH) and Clearwater Athabasca Spillway (CS) head choke-points discussed in the text are also shown.

leave a record) conspire to produce significant differences in the time variation of these proxies. The maximum strandline elevation, for instance, follows Lake Agassiz surface elevation variations more closely than lake depth variations at southern Lake Winnipeg. Maximum lake depth "maxfill" (also limited to maximum topographic relief) has even further divergent variations compared to the other synthetic proxies. These differences emphasize the caution required in making direct inferences from strandline observations and in comparing inferences based on spatially diverse sets of strandlines.

In comparing model results against past interpretations, it should first be noted that most strandlines cannot be traced very far, and nearly all are undated giving rise to a wide range of interpretations (e.g., Fisher, 2005). Inferred Lake Agassiz levels based on observed strandlines have been graphically summarized by Fisher and Souch (1998). Their lake-level chronology has a significant drop just after −10.8 ^{14}C ka (about −12.9 ka) to the low water "Moorhead" phase, a subsequent rise to the Campbell level at 9.9 ^{14}C ka (about −11.3 ka) and a subsequent final drop after either 9.5 ^{14}C ka (about −10.7 ka) or 9.3 ^{14}C ka (about −10.5 ka). These are all in close correspondence with the maximum strandline chronology of Fig. 10. However, their preferred variant has an additional lake-level drop and recovery during the "Emerson" phase between 9.9 ^{14}C ka and 9.5 ^{14}C ka . This is due to an inferred initial opening of NW drainage at 9.9 ^{14}C ka which does not occur in our model.

Comparison can also be made against the reconstruction of Teller et al. (2002), hereafter the TLM reconstruction, derived from a combination of strandline and isobase data using GIS technology. As shown in Table 4, the main discrepancy consists of a much larger drop during the −10.6 to −10.3 ka period in our ensembles. Given that the TLM reconstruction was only for the indicated time-slices, comparison is problematic for additional lake-level drops in the ensembles. The dates of the Norcross and Tintah

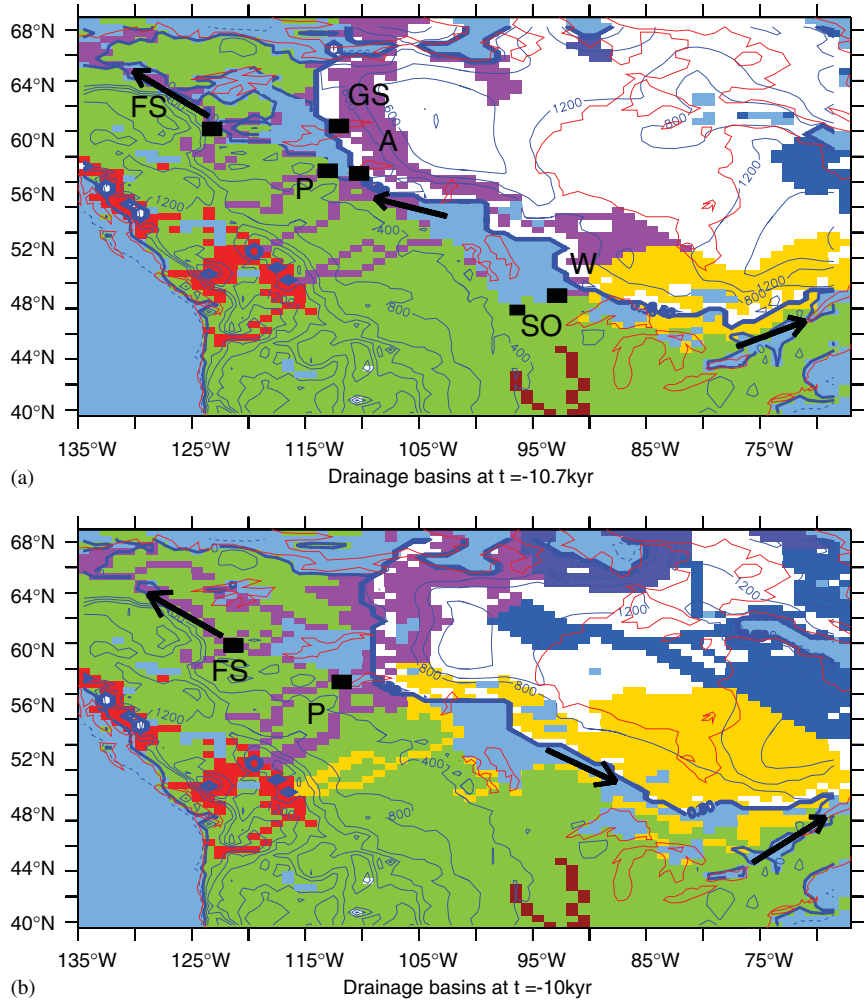

Fig. 9. Drainage basins at −10.7 ka "(a)" and −10 ka "(b)" for good fit run n1062. Drainage basin colour coding as for Fig. 6. Also shown are the locations of the Fort Simpson (FS), Great Slave (GS), Lake Athabasca (A), Peace River (P), Southern Outlet (SO), and Wampum (W) strandline and river delta sites.

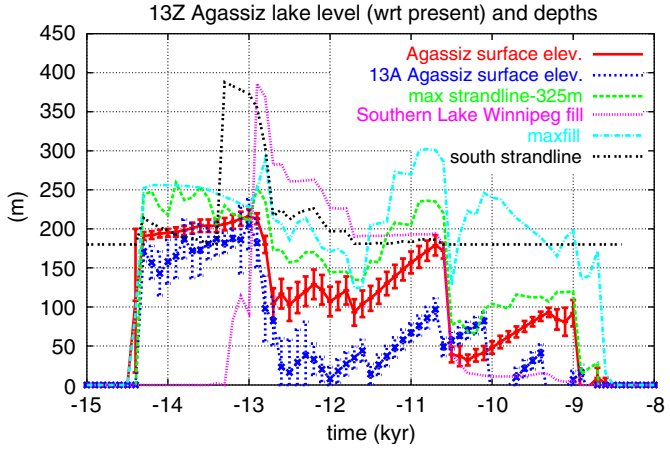

Fig. 10. Computed Agassiz Lake level proxies. Agassiz lake level is lake surface elevation above the present day sea-level datum. "Max strandline" is the maximum value of (lake depth [up to peak sub-grid topographic relief] + present day surface elevation). "Maxfill" is maximum model depth up to maximum sub-grid topographic relief. "southern Lake Winnipeg fill" (i.e. depth) is computed for the grid-cell at 96.5°W and 51.25°N. "South strandline" is located near the southern margin of Lake Agassiz at 96.5°W and 48.75°N and has 123 m subtracted from it.

stages are also controversial and poorly constrained (Teller and Leverington, 2004; Fisher, 2005). As such, we have shifted the modelled lake stage assignments in Table 4 to allow better sequential correspondence to the TLM reconstruction. For ensemble 13P, however, this shift might better have been imposed in the opposite time direction with assignment of the 29 m drop at −10.7 to −10.6 ka to the Tintah stage. The impact of hydrological tuning is also evident in the large post −11.7 ka difference in lake drop histories between the non-hydrologically tuned ensemble 13A and the hydrologically tuned ensembles (Table 4).

For testing and tuning of the Lake Agassiz sector of our chronology, we have relied on two sets of dates. The first set is 9.5 ^{14}C ka (approximately −10.7 ± 100 ka) from just below upper Campbell beach sediment in Minnesota at 302 m (Fisher, pers. comm.) located in the vicinity of the SO (96.35°W, 47.88°N, Fig. 9a). The second site ("Wampum", 92.85°W, 49.02°N, Teller et al., 2000) has 9.3–9.4 ^{14}C ka (about −10.5 to −10.6 ka) dates just under Campbell beach sediment and sits on the southeast margin of

Table 4
Lake drop comparison between ensemble mean values for southern Lake Winnipeg and "Lake Agassiz" values computed by TLM (Teller et al., 2002)

TLM lake stage	Timing (ka)		Mean drop (m)					
	TLM	Model	TLM	13Z	13G	13C	13P	13A
Herman	−12.9	−12.9:−12.6	110	104	74	78	93	88
		−12.6:−12.3		21	21	16	6	15
		−12.3:−12.2					3	16
Norcross	−11.7	−12.2:−12.0	52	36	31	41	26	43
Tintah	−11.2	−11.9:−11.7	30	36	30	39	40	39 (−11.5 ka)
		−10.8:−10.6		14	43		29	55
Upper and Lower Campbell and McCauleyville	−10.6:−10.3	−10.6:−10.3	56	165	157	134	155	7
Hillsboro	−10.0	−10.1:−10.	7	1		2		57
Burnside and The Pas	−9.5:−9.2	−9.5:−9.2	24	7	13	10	44	
		−9.0:−8.8			13		13	

Lake Agassiz (Fig. 9a). Our initial base ensemble 13A however has no inundation of either of these sites after −12.3 ka. Lake Agassiz outlet choke-points are far from RSL data points and for ensemble 13A are only subject to constraints provided by the transect of absolute gravity measurements which have significant uncertainties. The misfit has also made it apparent that the ensemble parameters provide inadequate phase-space coverage for this region. Therefore, to further constrain the Lake Agassiz chronology, regional precipitation and desert-elevation parameterizations were modified to allow a fit to the SO data. However, this was carried out by hand tuning and therefore is unlikely to produce an optimally calibrated ensemble. Future work will incorporate strandline data into the Bayesian calibration in order to ensure overall quality of fit to all constraint data.

We were able to tune the lower bound ensemble 13P so that its mean strandline elevation for the SO matched the observed value during the upper Campbell stage (Fig. 11). However, this was not the case for other ensembles with larger Keewatin domes. Ensemble 13G was tuned well within 1 sigma fit to the observations using extreme desert-elevation forcing over the NW choke-point region. Ensemble 13Z was obtained using what we judged to be a more reasonable value for regional desert-elevation forcing at the cost of a 10 m shortfall for 1 sigma fit. Ensembles 13A and 13C have no filling of the adjacent grid-cells for this period. With respect to the Wampum datum, ensemble 13P has flooding of the region until after −10.5 ka, while 13Z is flooded till after −10.6 ka, 13G till after −10.8 ka, and 13C has no flooding after −11.8 ka. Given that drainage routings are calculated based on surface topography at the end of the time-step, 13G flood termination of the Wampum site is within 1 sigma uncertainty of ^{14}C dates. In summary, ensembles 13G, 13P, and 13Z are within (or almost within) 1 sigma fit of the Lake Agassiz strandline data, while ensembles 13C and 13A do not at all fit the data given the margin chronology employed.

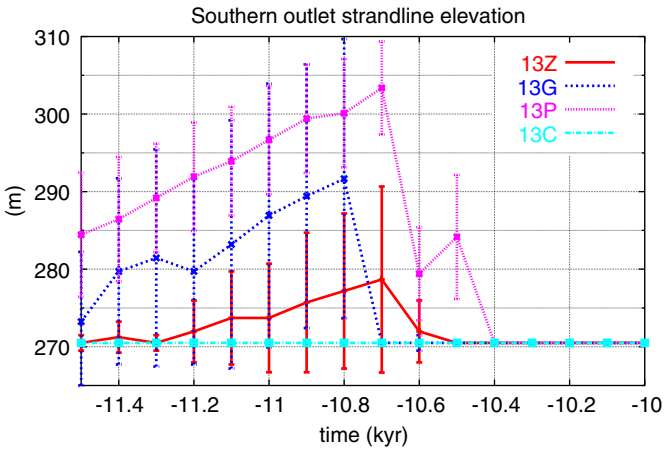

Fig. 11. Computed "strandline histories" for SO site (96.35°W, 47.88°N). These are defined as fill depth plus present day drainage elevation. Values are interpolated to the exact geographic latitude but use nearest neighbour value with respect to longitude.

In the model, Lake Agassiz starts after −14.5 ka (Fig. 12), about 700 years prior to past inferences of 11.7 ^{14}C ka (Fenton et al., 1983). It has only moderate volume for about a ka. A rapid increase in ensemble 13Z lake size from −13.4 to −12.8 ka is due to significant margin recession (Fig. 8). Subsequent lake volumes at times exceed the upper bound ("north") estimate of Leverington et al. (2002) as shown in Fig. 12. Furthermore, the ensemble lake volume chronology has much stronger variations throughout the period prior to Lake Ojibway. Some overestimation of lake area and thereby volume is to be expected in our model given its relatively coarse resolution. It is evident in Fig. 12 that most of the volume excess is related to the area excess. There is a large discrepancy during the post -9 ka stage, the latter part of which is due to earlier marine inundation (along the NW margin of Hudson Bay ice dome) of Lake Agassiz/Ojibway in the model (volumes and areas are only for fresh-water lakes).

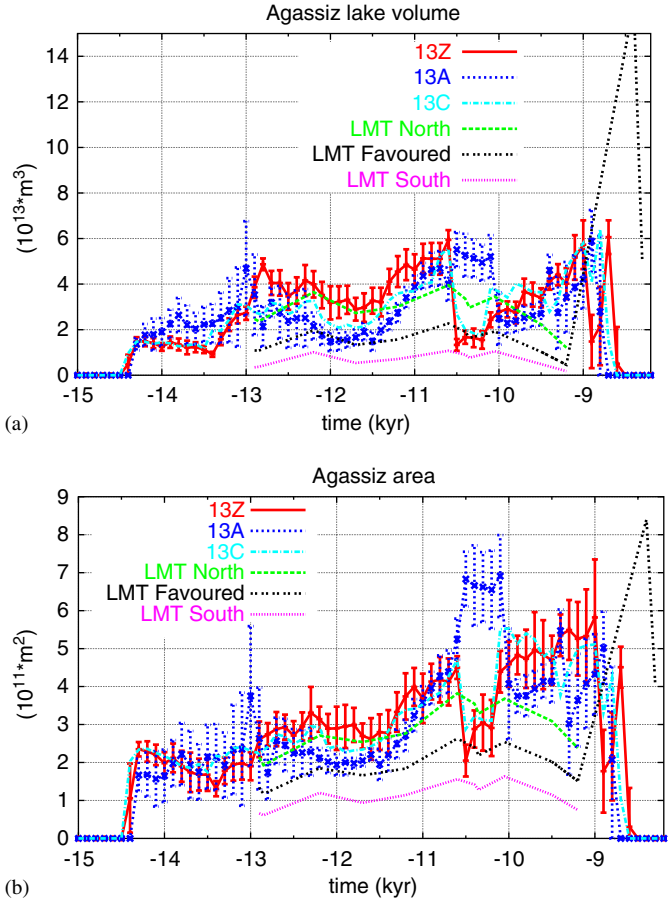

Fig. 12. Ensemble Lake Agassiz volume "(a)" and area "(b)" and estimates from LMT (Leverington et al., 2002).

It is curious that even ensemble 13A has significant Lake Agassiz area excesses relative to the upper bound reconstruction of Leverington et al. (2002), especially at the upper Campbell high stage around −10.7 to −10.6 ka. One would expect the opposite if anything, given that ensemble 13A has inundation of neither the Wampum nor the SO sites at this time, while the reconstruction of Leverington et al. (2002) is derived from strandline and isobase data. Given that the SO and Wampum sites delineate the southern and arguably eastern extent of the lake (Fig. 9a), the area excesses are likely restricted to the western and northern margins of the lake. Identifying the source of this discrepancy will require more field data to constrain these two different approaches to lake-level reconstruction.

Another interesting feature evident in Fig. 12 is the monotonic growth in lake area and lack of significant reductions in lake volume during the −12.9 to −12.6 ka period when a significant lake-level drop is predicted (Table 4). Large lake volume drops occur only after −10.5, −9.5, and −8.9 ka in correspondence with the lake-level drops shown in Table 4, along with the final collapse of the Hudson Bay ice dome after −8.5 ka. The relation of these drops to controlling choke-point elevations is discussed below.

Turning to the NW sector (i.e. glacial Lake McConnell), ensemble 13A also does not fit with maximum observed strandlines for the Athabasca, Great Slave, and Great Bear Lake regions (Table 5). For this region, initial ensemble constraints comprised two RSL data sites along the NW continental margin (not shown) and measured values for $\dot{R}$ at Yellowknife using VLBI. Assuming that the maximum observed strandline elevations correspond to the actual maximum level of deglacial flooding, the excessive strandline elevations computed for ensemble 13A indicates some combination of excessive ice load over the McConnell region and insufficient ice load for the Lake McConnell outlet. To remedy this, ensemble 13P was the most strongly tuned with increased precipitation over the outlet region along with a strong reduction in precipitation (and therefore ice loads) over the Great Bear to Lake Athabasca region. Furthermore, in order to generate sufficient LGM ice volume, precipitation was increased to the east of this region in order to force an eastward shift of the Keewatin dome. Precipitation modifications were also subject to the constraint of 1 sigma (i.e. ±1.55 mm/yr) agreement between model and measured values of Yellowknife $\dot{R}$.

Though good fits for maximum strandline elevations are obtained for Lake Athabasca and Great Bear Lake, ensemble 13P is still unable to fit the Great Slave Lake data. These results along with the minimal Keewatin ice load of ensemble 13P (as indicated by its lower bound mean value for Yellowknife $\dot{R}$ in Table 3) may suggest that the 320 m maximum Great Slave strandline elevation of Smith (1994) does not correspond to the maximum regional level of flooding during deglaciation. All ensembles had computed minimum Great Slave Lake strandlines above the maximum local sub-grid elevation indicating complete submergence of the site. Smith (1994) has also noted that raised beaches along the Canadian Shield are patchy and especially difficult to locate on the ground. The anomalous trend of Great Slave Lake strandline elevations rising and then decreasing to the east (Smith, 1994) may also either corroborate this suggestion or indicate a much more complicated regional deglaciation history than can be generated by the model as presently configured.

The Lake Athabasca site is the closest of the sites listed in Table 5 to the NW choke-point region for Lake Agassiz drainage and therefore the most important with respect to constraining Lake Agassiz drainage routing. As such, ensemble tunings to this strandline were chosen so as to bracket possible load histories for the NW choke-point region. Specifically, ensembles 13Z and 13C were tuned to 1 sigma agreement with the highest observed Lake Athabasca strandline. However, as mentioned above, the models were also tuned to a higher ice volume to better fit global ice-volume constraints. This was at the cost of a stronger misfit to the highest strandline elevation around Great Bear lake. On the other hand, ensemble 13G has a 1 sigma upper bound Lake Athabasca strandline elevation that is 13 m below that observed. This under-fit is due to the extreme desert-elevation forcing imposed in the vicinity

Table 5
NW strandline and dated lake delta elevation (m) comparison to model

Site	Max obs.	Time (ka)	13Z	13G	13C	13P	13A	Lat.	Long.
Athabasca	315	−13.3:−10.5	292 ± 24	281 ± 21	293 ± 34	319 ± 6	429 ± 57	58.67	110.27
Great Slave	320	−10.6	467 ± 55	469 ± 23	452 ± 84	391 ± 12	449 ± 16	62.42	112.04
Great Bear	298	−12.7/6	412 ± 42	426 ± 33	415 ± 44	307 ± 5	360 ± 42	66.64	118.33
Patuanak	500	−12.2	485 ± 20	481 ± 15	504 ± 3	465 ± 26	466 ± 23	52.2	107.8
Mtn.R.	93	−13.86:−13.51	125 ± 34	152 ± 29	120 ± 30	123 ± 25	163 ± 15	65.65	128.88
Litt.Bear	93	−13.81:−13.19	226 ± 8	239 ± 19	221 ± 5	206 ± 16	207 ± 15	64.88	125.67
Athabasca	236	−11.55:−11.20	283 ± 90	284 ± 87	291 ± 100	355 ± 76	296 ± 17	58.25	111.42
Peace 1	247	−11.30:−11.19	256 ± 18	254 ± 13	257 ± 20	327 ± 47	267 ± 8	58.88	113.03
Peace 2	223	−10.17:−9.60	237 ± 32	229 ± 22	240 ± 36	269 ± 57	240 ± 14	58.95	111.80
F. S. 1	128	−10.58:−9.92	104 ± 7	105 ± 3	107 ± 4	119 ± 16	115 ± 12	62.18	123.20
F. S. 2	136	−10.18:−9.50	150 ± 25	141 ± 23	142 ± 24	147 ± 22	131 ± 6	61.83	121.33

Strandline elevations for the first three sites are maximum observed (Smith, 1994) and maximum mean values from ensemble runs. The same applies to the fourth site but the data comes from Fisher and Smith (1994). Computed lake elevations for the remaining six sites are maximal mean range (plus 1 sigma) for the date range. Data for these six sites are also from Smith (1994). Dated samples were converted to 1 sigma calendar year ranges using CALIB 4.1 with INTCAL98 (Stuiver et al., 1998a). Locations are also shown for the nearest time-slice in Figs. 8 and 9.

of the NW choke-point required in order to maximize the fit to the southern Lake Agassiz strandline data presented above. Finally, ensemble 13P is the most strongly tuned to the strandline data-set and represents a lower limit (likely excessively) deglacial Keewatin ice load history.

Calibrated ^{14}C dates for regional river and lake deltas from Smith (1994) are also shown in Table 5. Elevations of samples from lake deltas only provide a minimum elevation for the height of inundation. Aside from Fort Simpson sample # 1 (F.S. 1 in Table 5), all ensembles predict mean lake surface elevations that are above these river delta surface elevations (with the small exception of ensemble 13A for site F.S. 2) during the calibrated date range and are therefore consistent with these observations.

For its duration, glacial Lake McConnell incorporates 5–60% of the total lake volume in our model (Fig. 13). Inception of Lake McConnell is poorly defined as the region has small proglacial lakes going back to at least −15.2 ka. However, a significant lake starts to develop around −13.9 ka (Fig. 13). Termination of the lake varies widely across runs as is evident by the large 1 sigma scatter for ensemble 13Z in Fig. 13. Considering the ensemble mean, termination occurs after −9.5 ka. As such, lake duration is in reasonable agreement with the 11.8 ^{14}C ka (−13.8 ka) to 8.3 ^{14}C ka (−9.4 to −9.3 ka) span inferred by Smith (1994). The impact of strandline tuning on modelled Lake McConnell is also evident in Fig. 13 with significant differences between the strandline tuned ensemble 13Z in comparison with the base ensemble 13A.

Some runs with larger Keewatin ice domes have large repeated marine inundations of the Lake McConnell region resulting in the 0 volume episodes of the lower 1 sigma scatter in the volume chronology. The −12.8 ka drainage basin snapshot for run nn1062 in Fig. 8b provides an example of such inundation. Much larger inundations that completely flood the Great Slave Lake region happen around −10 ka in some relatively high scoring model runs (not shown). Field examination for RSL data in the

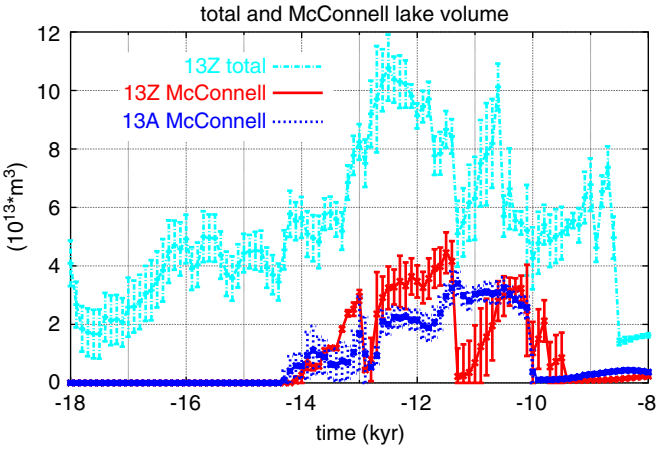

Fig. 13. Total and McConnell (freshwater) lake volume chronologies. The total value includes all North American freshwater lakes on the model grid (i.e. north of 34° latitude.)

Keewatin region could provide some much improved constraints for deglacial ice thickness in this region.

For an examination of the eastern drainage sector, we show computed Lake Michigan and Lake Huron levels in Fig. 14. It should be noted that none of the ensembles has been tuned to data from the Great Lakes sector. Our reconstructed lake-level history for the southern Lake Michigan basin has chronological correspondence to the inferred history of Colman et al. (1994a) (shown in the figure), but amplitudes of lake-level variations are only in partial agreement. Further validation for the chronology is evident when compared against δ^{18}O records for the southern Michigan basin (Colman et al., 1994b) which has two significant low δ^{18}O pulses. One occurs sometime between −14 ka and YD onset and a second pulse with split peaks is at about −10.05 ± 0.1 ka (8.9 ^{14}C ka) and −9.6 ka (8.6 ^{14}C ka). These pulses could correspond to the −13.2 and −9.6 to −9.1 ka periods of initial inundation

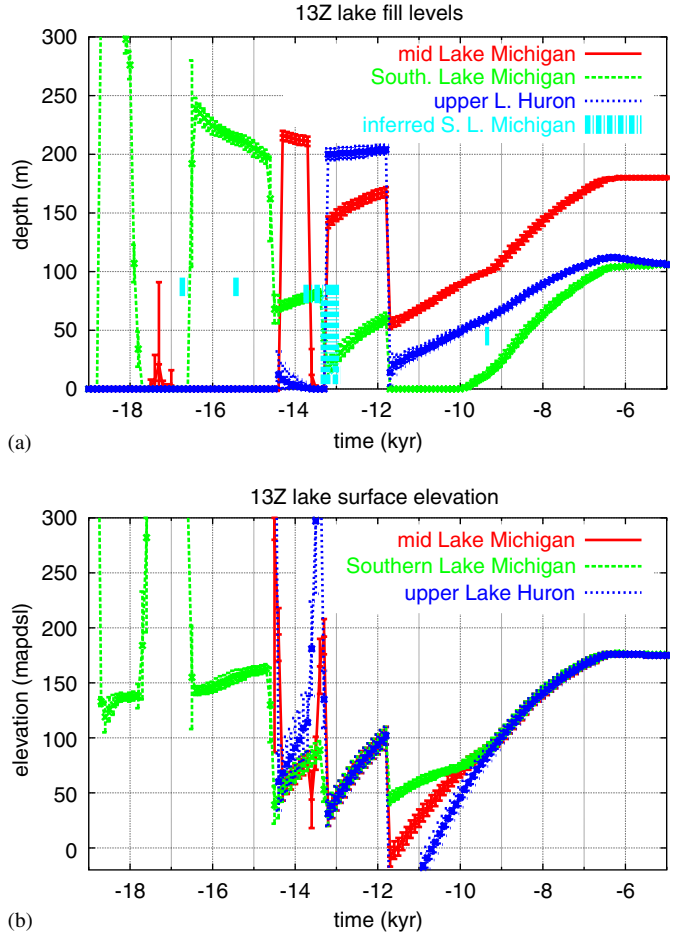

Fig. 14. Computed lake fill levels (i.e. depths) "(a)" and lake surface elevations (above present day sea-level datum) "(b)". Geographic coordinates for the mid and southern Lake Michigan and upper Lake Huron sites are respectively: (86.5°W, 44.75°N), (87.5°W, 42.75°N), (82.5°W, 45.25°N). The inferred southern Lake Michigan data is from Colman et al. (1994a).

evident in Fig. 14 when isotopically depleted meltwater from Lake Huron could have entered the basins.

Overall, we have shown a reasonable fit of the hydrologically tuned ensembles 13Z, 13P, and 13C to our set of proglacial lake proxies given data uncertainties. Our most significant misfit is the apparently excessive maximum strandline elevation computed for Great Slave Lake. Models that respect the $\dot{R}$ data for Yellowknife are unable to deliver the shallow paleo depths indicated by the strandline data. Improvements on the error bounds for the $\dot{R}$ data along with a re-examination of the region for possibly higher strandline elevations will hopefully resolve this discrepancy. Having, thus tested the ensemble results against available data, consideration of the controversial issue of the drainage routing history of Lake Agassiz is in order.

3.3. Lake Agassiz routing history

In agreement with past inferences (e.g., Teller et al., 2002; Fisher, 2003), our analyses indicate that the southward drainage of Lake Agassiz terminates around the onset of the YD (Fig. 5b). The ensemble using the delayed margin forcing chronology 13S has the latest shutdown at −12.6 ka, while most other ensembles shut down the SO after −12.9 ka except for 13C which shuts down after −13.0 ka. As previously discussed, this portion of the chronology of ensemble 13S is disqualified during the early YD interval on the basis of proxy records from sediment cores near the mouth of the Mississippi River, which indicate shutdown of significant Mississippi outflow by −10.8 ^{14}C ka (−12.9 ka).

At −12.8 ka, there is strong sensitivity of the ensemble meltwater routing distribution to the width of the margin buffer. The three ensembles (13A, 13C, and 13G) with a ±100 km margin buffer are characterized by almost all model runs having an active NW outlet for Lake Agassiz while the remaining ensembles have less than 10% of runs with an active NW outlet (Fig. 15a). This divergent behaviour is due to a 1 grid-cell wider margin buffer north of Wapawekka Hills ("WH" in Fig. 8b) in the ±100 km margin buffer chronology that reduces the ice flux to the grid-cell covering Wapawekka Hills and thereby allows ice-free conditions at the grid-cell during the −12.89 to −12.8 ka drainage time-step. Fisher and Smith (1994) and Fisher and Souch (1998) have also discussed the critical impact of uncertainties in the ice-margin chronology around Wapawekka Hills on drainage routing. As such, a detailed field investigation of the northern margin of the Wapawekka Hills (Rayburn, 1997) would hopefully constrain the choice of margin chronologies. However, in spite of the lack of Lake Agassiz drainage basin outflow to the NW, ensemble 13Z suffers only a 0.06 dSv reduction in −12.8 ka meltwater (and iceberg) discharge into the Arctic in comparison to the ensemble 13G (Fig. 7b). Removal of the 2 model runs in 13Z that do have NW drainage of Lake Agassiz during −12.8 ka results in only a 0.005 dSv reduction in the weighted mean Arctic discharge for that timestep. Regional NW (i.e. McConnell drainage basin) melting and ice calving therefore strongly dominates overflow from the Lake Agassiz drainage basin during this time-step.

At −12.1 ka, the NW outlet then dominates Lake Agassiz drainage in all ensembles until the Upper Campbell high-water stage, which in the model occurs between −10.7 and −10.6 ka (Fig. 15a). Intervals when all runs have identical routing of Lake Agassiz outflow (i.e. when ensemble routing fractions are 100% across ensembles in Fig. 15a) are taken to express high confidence (though still subject to uncertainties with the margin forcing chronology). The −11.9 to −10.8 ka interval has 100% NW routing of Lake Agassiz drainage for all ensembles (Fig. 15a) except for the delayed margin forcing ensemble 13S, which has 100% NW routing over the −11.7 to −10.4 ka interval. The complete ensemble shutdown of NW drainage through the Mackenzie River basin between −10.7 and −10.5 ka (aside from ensemble 13S) is in close agreement with the 9.45 ^{14}C ka best estimate of Fisher

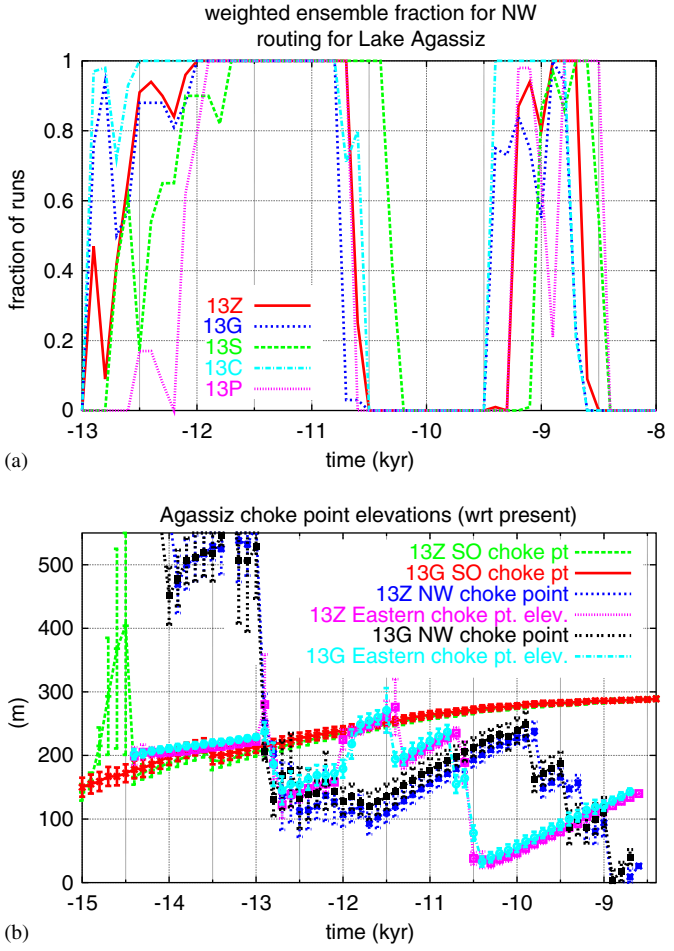

Fig. 15. Calibrated (i.e. RSL fit weighted) fraction of ensemble runs with NW drainage of Lake Agassiz as a function of time "(a)" and computed Lake Agassiz choke-point surface elevations "(b)". The choke-point locations are dynamically computed by the drainage solver. The lowest choke-point at any time is the contemporaneous outlet. The ensembles are described in Table 3.

(2005a). From −10.5 to −9.5 ka, all runs in the three hydrologically tuned ensembles (13Z, 13G, and 13P) have eastern routing of Lake Agassiz outflow. By −9.2 ka, drainage routing for the final stage of Lake Agassiz/Ojibway is again largely to the Arctic Ocean, but this time along the margin of the ice sheet and therefore to the northeast of the Mackenzie River basin.

It is worth noting that the drainage routing chronology obtained in the ensembles is in only partial agreement with that assumed in the construction of the margin forcing chronology (Dyke, 2004). The latter has eastern drainage during the −12.7 ka time-slice, NW drainage during the −12 and −11.5 ka time-slices, southern drainage during the −11 and −10.75 ka time-slices, followed by eastern drainage via glacial lakes Nipigon and Ojibway.

The robustness of Lake Agassiz drainage routing in the ensembles can be further examined via the comparison of elevation chronologies for the NW, southern, and eastern choke-points shown in Fig. 15b. It is clear that the SO is completely inaccessible after −12.9 ka for ensemble 13G

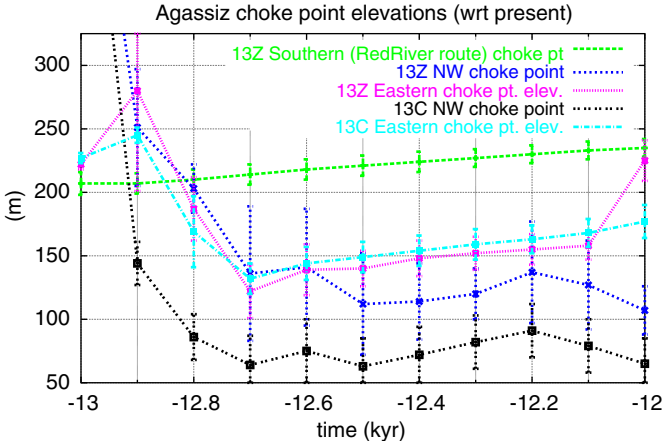

Fig. 16. Expanded version of ensemble Lake Agassiz choke-point surface elevations from Fig. 15b.

and after −12.8 ka for ensemble 13Z. Furthermore, after −12.1 ka, the weighted eastern choke-point elevation for ensemble 13Z is greater than two standard deviations above that of the NW choke-point until −10.7 ka. The increasing elevation of the eastern choke-point from −12 to −11.5 ka is largely due to the "Marquette" readvance of ice across Lake Superior. The generally large differences between eastern and NW choke-point elevations also imply that the approximately 5 m uncertainty in the MDhby drainage topography is insignificant with respect to the computed 13Z Agassiz outlet routing for the −12.1 to −10.5 ka interval. On the other hand, the Agassiz outlet chronology is much more uncertain during the early YD interval. The −12.7 to −12.0 ka interval represents a long single time-step of the margin chronology during which the drainage calculation interpolates sub-grid margin recession across the NW choke-points. The drops in NW choke-point elevation during the −12.2 to −12.1 ka and −12.1 to −12.0 ka intervals (Fig. 16) are due to imposed drops in the elevation of the head of the Clearwater Athabasca Spillway (indicated as "CS" in Fig. 8) in the model drainage topography, which are weakly constrained chronologically based on interpolated margin recession across the sub-grid (i.e. high-resolution) drainage topography. This source of uncertainty along with the oscillating and mostly less than 30 m weighted mean elevation difference between eastern and NW choke-points for ensemble 13Z (Fig. 16) during the −13.0 to −12.1 ka interval suggests that definitive drainage routing determination will need much stronger model calibration and higher temporal resolution of the margin chronology during this period (and therefore more field data).

The possibility of a dominant NW outlet during the YD and especially during its onset has until recently received little consideration in the literature. In spite of the aforementioned Gulf of St. Lawrence and Lake Champlain salinity reconstructions, most interpretations (e.g., Teller, 2001; Dyke, 2004) assume an eastern outlet during the Moorhead low-water phase of Lake Agassiz that began

between −12.9 and −12.8 ka with only a few exceptions. Karrow (2002) cites a number of past studies that have considered a NW outlet including that of Minning et al. (1994) who concluded that the NW outlet was the "most probable outlet for the Moorhead phase". Teller et al. (2005) and Lowell et al. (2005) have also questioned eastern drainage during this time on the basis of the absence of coarse flood gravel deposits along with the morphology of possible drainage channels in the Thunder Bay region and doubts about the assumed chronology of deglaciation. A key region for constraining Lake Agassiz routing during the early YD is around the head of the Clearwater Athabasca Spillway (CLAS) which is shown as "CS" in Fig. 8b. The CLAS channels the −12.8 ka NW outflow from Lake Agassiz in the model (at least for the handful of runs examined in detailed). Fisher and Smith (1994) also present extensive evidence for glacial drainage through the spillway, though they argue for initial opening of the spillway at 9.9 ^{14}C ka (about −11.3 ka) based on the youngest of 4 radiocarbon dates from wood and peat samples in flood gravel at the head of the spillway. It should be noted that two of the wood samples have 10.31 ± 0.29 and 10.015 ± 0.32 ^{14}C ka radiocarbon dates which translate to −12.81 to −11.34 ka and −12.31 to −11.16 ka one sigma confidence intervals under CALIB4.1 conversion. These dates are therefore consistent with ice-free conditions around the choke-point region during the early to mid YD interval. It is also possible that prior flow occurred, but all evidence for this was erased by the younger flow (Teller et al., 2005).

Maximum upstream strandline elevations for the CLAS region offer a further indirect test of our model routing chronologies during the early to mid YD. For the grid-cell covering Patuanak (shown as "PA in Fig. 8b and just to the south-east of the head of the CLAS), strandline elevations from Fisher and Smith (1994) range up to 500 m with a number of strandlines in the 490–500 m range. It should be noted that these high strandlines have been inferred to have formed around local lakes (Fisher and Smith, 1994). However, at least in all the best-fit runs that we have examined in detail, the strandlines are associated with NW outflow from Lake Agassiz. Ensembles 13C and 13Z cover the Patuanak region strandline elevation range (occurring between −12.4 and −12.1 ka) within one standard deviation with 13C having the highest weighted mean maximum strandline elevation of 504 m (Table 5). Ensembles 13A and 13P have slightly lower maximum strandlines for this grid-cell, with respect to one sigma upper bounds of 489 and 491 m. As such, these four baseline ensembles are reasonably consistent with the maximum strandline elevations for the region.

The diversion of Agassiz outflow from the south at about 13 ka is clearly indicated in the planktonic foraminifera δ^{18}O record from Orca Basin sedimentary cores (Broecker et al., 1989) but has largely been attributed to an eastward diversion of Agassiz outflow. A number of proxies such as percentages of reworked calcareous nanofossils in Orca Basin sediments (Marchitto and Wei, 1995; Brown and Kennett, 1998) also indicate that meltwater was permanently diverted from the Mississippi basin after onset of the YD. However, Fisher (2003) presents ^{14}C dates from a gravel horizon located near the approximate drainage divide of the southern spillway that are interpreted to indicate a second brief occupation of the SO that terminated no later than 9.4 ^{14}C ka (about −10.6 ka). Given the large elevation difference between the southern and NW choke-points during the −12.0 to −10.6 ka interval for our base 13Z and 13C ensembles (Fig. 15), late southern discharge would require modification of the ice-margin chronology employed in the model. A brief southern drainage event is also much more plausibly associated with a short-term surge-type readvance temporarily blocking an active outlet than with a switchover between eastern and western outlets. Thorleifson (1996) has suggested that there was a 10 ^{14}C ka (some time between −11.5 to −11.3 ka) ice re-advance into the Wapawekka Hills region and also to Riding Mountain and the south end of Lake Manitoba. Such a re-advance would have blocked NW outflow. Furthermore, the date for this inferred re-advance is during the peak of the Marquette re-advance of ice into the Lake Superior region during which the eastern choke-point elevation was higher than that of the SO (−11.8 to −11.4 ka in Fig. 15, with the highest elevation difference around −11.5 to −11.4 ka). Therefore a western Manitoba ice re-advance around −11.5 ka is the simplest margin chronology modification for the model that could produce a post YD southern discharge. As has been inferred by Teller (2001), a final retreat would then have occurred soon after this thereby initiating a large flood into the NW consistent with the 9.9 ^{14}C ka (about−11.3 ka) estimate for such a flood by Fisher and Smith (1994) based on dated flood gravel. This date for a NW flood in combination with evidence for the lack of SO inundation during the 10.23 ^{14}C ka to 9.92 ^{14}C ka interval (based on ^{14}C dated macro-fossils indicative of deciduous parkland forest, Yansa and Ashworth, 2005) along with the −11.8 to −11.4 ka model window in Fig. 15 would imply that such a southern discharge could only have happened briefly some time after −11.5 ka and before −11.3 ka. Based on moraines and ice flow indicators, Thorleifson (1996) also argues that this Manitoba re-advance involved very thin ice which would be dynamically difficult to sustain over any significant length of time, especially in the presence of rising lake levels. A longer term southern discharge event would also be difficult to reconcile with the Orca Basin data discussed above that indicate complete shutdown of Mississippi discharge after YD onset.

The only other opportunity for post YD southern discharge without significant modifications to the margin chronology would be during the upper Campbell stage around −10.7 ka. This would also fit well with dates from the youngest flood gravel horizon in sediment cores from the SO (Fisher, 2003). But as is evident in Fig. 15, this

would again require ice blockage of NW drainage. And this would entail an ice re-advance somewhere NW of Wapawekka Hills given the extent of Campbell beach shorelines (e.g., as shown in Schreiner, 1983). Teller and Leverington (2004) appear to impose such an ice re-advance in their Post Tintah to Upper Campbell transition during which they have Lake Agassiz drainage change from NW to southern outflow. The 20 m shortfall in the mean elevation of the eastern choke-point relative to that of the southern chokepoint arguably lies within model uncertainties. A point in favour of such an event is the difficulty that we had in tuning large ice-volume ensembles to fit the upper Campbell strandline data discussed above. Ice blockage of NW drainage would obviate the need for such tuning.

4. Discussion: drainage history impact on climate

During the mwp1-a interval from −14.6 to −14.0 ka, meltwater discharge variations are (to the 100 year temporal resolution of the drainage module) synchronous with the GRIP δ^{18}O climate forcing chronology (Fig. 17). One may speculate that increasing meltwater discharge into the Arctic and Atlantic Oceans resulted in a negative feedback which helped terminate the warmest phase of the B–A. However, the existence of a ^{14}C plateau during this period (Stuiver et al., 1998a) along with the uncertainties evident in the phase spread between the GRIP and GISP II δ^{18}O chronologies and the large time-steps in the margin chronology covering this interval (Table 1) leaves phase relationships uncertain. Resolution of the role of meltwater discharge during the mwp1-a interval must await the development of more detailed and independent chronologies.

Considering the next climatic oscillation, the largest meltwater pulse into the Arctic Ocean (at −12.9 to −12.7 ka) is coincident with the GISPII depiction of YD onset and slightly leads the YD onset indicated in the GRIP δ^{18}O chronology (as shown in Fig. 17). This, along with the robustness of this discharge across all but the 13S ensemble suggests that Arctic discharge may have played a key role in initiating the YD. Comparing δ^{18}O climate proxies for the mwp1-a and YD onset periods against meltwater discharge magnitudes from the various geographic sectors in Fig. 17 suggests that the THC is much more sensitive to Arctic discharge than to Atlantic discharge (Tarasov and Peltier, 2005). In accord with this hypothesis, subsequent meltwater (and iceberg) pulses into the Arctic Ocean may have been critical to maintaining THC shutdown for the full duration of the YD. It is also possible that iceberg discharge out of Hudson strait (i.e. H0 after −12.0 ka in Fig. 3b) may have also played a role in maintaining THC shutdown. However, the more limited spatial extent of its signature would raise questions as to whether such discharge could significantly impact NADW formation in the GIN sea region.

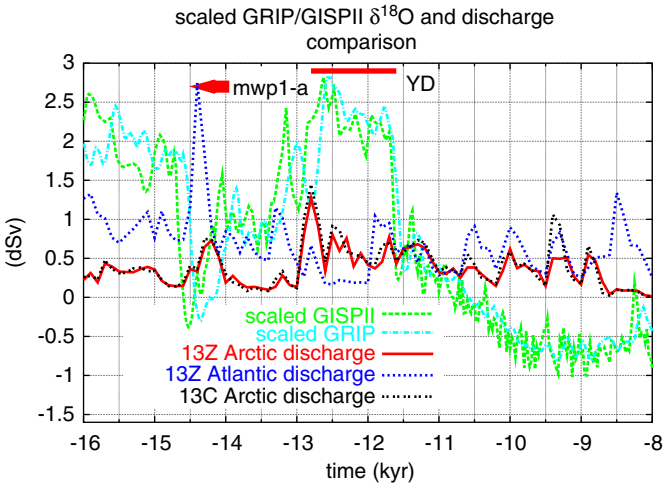

Fig. 17. Scaled GRIP and GISPII δ^{18}O records with Arctic and total Atlantic Ocean (South-east Ellesmere to Gulf of Mexico) discharges.

Though a detailed dynamical understanding of the impact of increased meltwater discharge into the Arctic is lacking, a rough conceptual picture is available. Previous analyses have concluded that deep ocean convection in the GIN seas region is very sensitive to changes in fresh-water influx and that this influx from the Arctic Ocean "ultimately controls" GIN seas ventilation (Aagaard and Carmack, 1989). The strong salinity stratification of the Canadian Arctic Basin (Aagaard and Carmack, 1989) along with reduced air–sea fluxes due to sea-ice cover would be expected to more easily preserve a freshened surface layer than is suggested by our analyses for the Atlantic. Such a freshwater cap would then be exported through Fram Strait via the East Greenland Boundary current which is the main present day export route for the Arctic Basin (Aagaard and Carmack, 1989) and was the only export route during the YD. However, it has also been inferred that the upper layers of this boundary current are presently nearly isolated from the convective regions of the GIN Seas (Aagaard and Carmack, 1989). Though a large glacial increase in meltwater flux may have disrupted this isolation, it is also possible that indirect feedbacks were also involved. For instance, Fisher et al. (2002) have speculated on dynamical feedbacks associated with increased pack ice due to enhanced Arctic meltwater discharge in the context of a dynamical source for the Preboreal Oscillation (PBO) that began at −11.3 ka. Thicker pack ice could have supported a stronger and more persistent anticyclone over the Arctic Basin, producing stronger winds and currents to increase sea-ice flux out of Fram Strait and into the region of NADW formation. Present day freshwater inputs into the whole Arctic basin (runoff and precipitation–evaporation) are about 1.3 dSv with runoff from the Mackenzie Basin contributing only 0.11 dSv (Aagaard and Carmack, 1989). As such, the order 1–2.5 dSv discharge into the Arctic Ocean computed by our model would have significantly increased both the flux of upper layer freshwater and sea-ice into the East Greenland current.

Current sea-ice fluxes out of the Arctic Ocean suggest that increased sea-ice production and export may have been the main mode for Arctic YD discharge impact on NADW formation. Sea-ice export through Fram Strait presently represents two-thirds of mean annual freshwater export (0.9 dSv) from the Arctic Ocean (Aagaard and Carmack, 1989). Furthermore, as a likely better analogue for mean annual YD conditions, mean monthly present day discharge during the winter months are at times greater than 2.4 dSv (Vinje et al., 1998). The iceberg component of NW discharge for ensemble 13Z is at least 0.2 dSv during the −12.89 to −12.8 ka timestep and thus represents a much smaller but still substantial contribution that would have survived transport to the surface of the GIN Seas.

Some further support for regional sea-ice expansion during the early YD can also be found on the basis of geomorphology. Dyke and Savelle (2000) have inferred slow ice-margin retreat on Victoria Island (just north of the Mackenzie basin) during the YD period and on this basis have hypothesized regional cooling during this interval. Enhanced sea-ice cover over the adjacent Beaufort Sea on account of our inferred large meltwater flux could have provided the basis for this regional chill.

Subsequent climatic oscillations provide possible further support for the concept of strong THC sensitivity to Arctic discharge. The termination of the YD at −11.6 ka is followed by the Preboreal oscillation (PBO) evident in the δ^{18}O records at approximately −11.4 to −11.3 ka. These two events correspond to respective local minima and maxima of Arctic discharge in Fig. 17 (subject to the uncertainties in the ice-margin chronology). However, given the previously discussed evidence for a short post YD interval of southern drainage of Lake Agassiz, we favour the hypothesis that an ice readvance in western Manitoba during the termination period of the YD would have further reduced Arctic discharge which could have aided resumption of interglacial NADW formation. Furthermore, as hypothesized above, final retreat of ice from Wapawekka Hills and western Manitoba could have initiated the 9.9 ^{14}C ka flood into the NW that has been hypothesized by Fisher et al. (2002) to have triggered the PBO.

A final climate oscillation recorded in the δ^{18}O records around −8.2 ka has been linked to the final collapse of the Hudson Bay ice dome at approximately −8.45 ka when Lake Agassiz (and Ojibway) water flooded into the Bay (Barber et al., 1999). Ensembles 13Z and 13C produce about a 1.6 dSv meltwater (and iceberg) "pulse" (as usual over a 100 year time-step) into the Labrador Sea during this collapse (Fig. 3b). The actual outburst flood from the release of the ice dammed Lake Agassiz/Ojibway would have occurred on an order 1 year time scale. It should also be noted that Clarke et al. (2004) provide a strong argument for subglacial release of the lake water. The greater than 100 year lag time between this pulse and the inferred climate oscillation is likely attributable to either an underestimated local carbonate reservoir effect or to a two-step model for final Lake Agassiz drainage into Hudson Bay (Leverington et al., 2002; Teller and Leverington, 2004).

As is clear from the Arctic discharge sensitivity to the ensemble variant 13S with modified margin chronology (Fig. 7b), margin chronology uncertainties imply that further constraints are needed to resolve the detailed phasing between meltwater discharge and climate response. For the case of the PBO, Fisher et al. (2002) provide ^{14}C dated samples to constrain the timing of Lake Agassiz discharge into the NW. For the case of the YD onset, a half-step delay in the margin chronology does not allow shutdown of southern discharge by −12.8 ka (as is evident with ensemble 13S in Fig. 5b), contrary to evidence from ^{14}C dated samples in lake mud (Fisher, 2003) extracted from the bottom of the SO spillway. Ensemble 13S does however impose synchronous delays across the whole margin and we cannot therefore rule-out regional modifications to the margin chronology. Future validation of the model against a larger set of dated Lake Agassiz strandlines and other paleo proxies will reduce uncertainties.

The initial challenge to the hypothesis that meltwater discharge via Gulf of St. Lawrence triggered the YD (Broecker et al., 1989) came from the consideration of the eustatic sea-level record inferred from dated Barbados corals (Fairbanks, 1989). The existence of the large mwp1-a event without a concurrent YD-type climate response, along with the lack of a similar meltwater pulse during the YD onset period remains a key constraint for interpretations of the cause of the YD. In this context, ensemble ice-volume histories are shown in Fig. 18. Our calibrated model produces a relatively narrow range of NA contributions to eustatic sea-level changes. The mwp1-a contribution for the lower bound ensemble 13P is 7.8 ± 0.2 m. The mwp1-a contribution is 8.7 ± 0.4 and 9.4 ± 0.3 m eustatic, respectively, for the hydrologically tuned 13Z and 13G

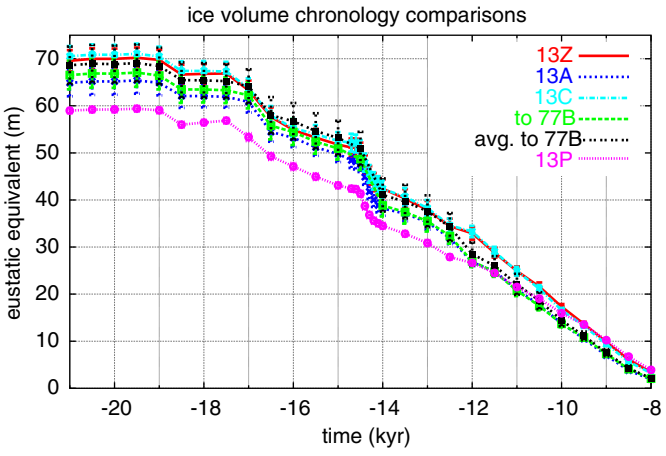

Fig. 18. North American ice-volume chronology and one sigma confidence intervals for various ensembles described in text.

ensembles, and 9.6 ± 0.3 m for the "upper bound" 13C ensemble (Table 3). The contribution is slightly larger for ensemble runs that were not subject to hydrological tuning. The non-hydrologically tuned base ensemble 13A has a contribution of 9.9 ± 0.3 m. The "to 77B" chronology is for a set of 1700 prior runs and has a mwp1-a contribution of 9.8 ± 0.3 m. Ensemble values for mwp1-a contributions arguably represent a lower bound estimate, especially since all the ensembles may have insufficient LGM ice volume given global constraints and contributions from other ice sheets (Peltier, 2004). A larger mwp1-a contribution could also have occurred if stronger large-scale ice-surging than represented in the model moved large quantities of ice into ablation and ice-calving regions.

It is also evident in Fig. 18 that in accord with observations, none of the ensembles produces a sharp eustatic meltwater pulse during the YD onset period. Likewise, none of the ensembles show a significant contribution to mwp1-b (approximately −11.4 to −11.1 ka).

The above results raise the question of the dynamical source for the approximately 10 m eustatic remainder of the contribution to mwp1-a. Arguments pointing to Antarctica as the dominant (Clark et al., 1996) or a significant (Clark et al., 2002) contributor to mwp1-a have largely been invalidated (Peltier, 2005). Arguments for a dominant Antarctic source, for instance, avoid the climatological issue that warming over Antarctica would have increased net accumulation over East Antarctica (where even at present melting is negligible). Indeed, 3D dynamical models of the Antarctic Ice Sheet predict no significant decay until approximately −10 ka (Denton and Hughes, 2002; Huybrechts, 2002). The key uncertainty which present day models cannot fully address is the possibility of a large-scale dynamical instability of the West Antarctic Ice Sheet (WAIS) (Oppenheimer, 1998) and/or marine components of an expanded East Antarctic Ice Sheet in response to rising sea levels.

Observational constraints on Ross Sea deglaciation (Conway et al., 1999) and analyses of marine cores from the northern Weddell (Cofaigh and Dowdeswell, 2001) appear to rule-out such an event for at least those sectors. Ocean dynamical arguments in favour of a significant Antarctic mwp-1a contribution (Weaver et al., 2003) also confuse freshwater flux with eustatic sea-level change. Rising sea levels would likely have caused some breakup of Antarctic ice-shelves which would have increased the freshwater flux into the Southern Ocean with no direct impact on eustatic sea level. Past model-based analyses have also shown the strong sensitivity of Eurasian ice sheets to climatic forcing (Tarasov and Peltier, 1997) and as such, it is likely that Eurasia contributed most of the remainder to mwp1-a. This assertion finds further corroboration in the new Eurasian deglaciation chronology of Saarnisto and Lunkka (2005) based upon the work conducted in the QUEEN program which suggests that the Barents Sea Ice Sheet was eliminated during the mwp1-a interval.

5. Conclusions

Based on glacial model ensemble runs, calibrated against a large set of RSL and geophysical constraints, further tuned to a set of geographically disperse strandline data, and forced with the best ice-margin chronology available, we have derived a surface meltwater drainage chronology for the deglaciation of the NA ice complex. Within dating uncertainties the chronology is consistent with $\delta^{18}O$ proxy records for Mississippi outflow. We find the NA contribution to mwp1-a to be approximately within the range of 7.7–10.2 m eustatic equivalent across a set of ensembles. Improvements in the confidence interval for the present day rate of vertical uplift at Yellowknife along with field collection of Keewatin region RSL data (and other constraints for sub-regions of Keewatin that did not experience marine inundation) could play a key role in reducing the uncertainty of the NA contribution to mwp1-a as it is the amount of ice over the Keewatin region that is least constrained in the model. Furthermore, no significant contribution to mwp1-b is found, indicating that a different ice sheet (likely Antarctica, as assumed in the construction of the ICE-4G (Peltier, 1994, 1996) and ICE-5G (Peltier, 2004) models) was a primary dynamical source of this event.

Our most significant result is the large, order 1–2 dSv over 100 year, meltwater discharge into the Arctic Ocean (largely via the McKenzie River outlet) at −12.8 ka, approximately coincident with the onset of the YD. This is also the largest deglacial meltwater pulse that the model predicts to have been delivered to the Arctic Ocean. Furthermore, our analyses favour an ensemble that has a NW outlet for Lake Agassiz during this pulse, as eastern outflow results in relatively large discharge into the Gulf of St. Lawrence that is contradicted by observations (ensemble values are 0.5–0.7 dSv meltwater/iceberg and up to 1.4 dSv including poorly constrained precipitation over ice-free land). Though not conclusive, NW drainage of Lake Agassiz during the YD is however not supported by the limited field data available (Lowell et al., 2005). As such, it is important to note that exclusion of all runs with NW drainage of Lake Agassiz at −12.8 ka from ensemble 13Z still produces a weighted mean (meltwater/iceberg) Arctic discharge of 1.2 dSv over 100 years which is still more than a factor 2 larger than the mean eastern discharge of 0.5 dSv for this modified ensemble. As such, ensemble results do not require a NW outlet for Lake Agassiz to produce a large YD onset pulse in the NW. Reduction of the large Keewatin ice dome produces a much larger meltwater flux during this period than the contribution from the Lake Agassiz drainage basin. The importance of a large Keewatin dome in combination with objective calibration of the GSM using a large set of paleo constraints is evident in the lack of significant YD Arctic discharge in previous studies (Licciardi et al., 1999; Marshall and Clarke, 1999) that lacked both of these attributes. These past works inferred substantial Arctic discharge only after termination of the YD.

The physical mechanism for the strong reduction of the Keewatin dome during YD onset can at this stage only be speculated upon. It may be related to the issue of why the dome only formed so late in the glacial cycle (Dyke et al., 2002). One possibility we offer is the displacement or switching of a "super-chinook" arising from the impact of the large Cordilleran Ice Sheet on a displaced jet stream. Dynamical destabilization of the warm-based Keewatin ice dome with resultant large-scale calving into adjacent pro-glacial lakes is another possible component.

The results presented herein, in combination with the isotopic records of sedimentary cores from the NW GIN Seas, support the hypothesis that the reorganization of the THC, which has become accepted as the cause of the YD was triggered and possibly sustained by meltwater discharge into the Arctic Ocean (Tarasov and Peltier, 2005). As such, these results also challenge the paradigm that deglacial floods large enough to influence climate were predicated upon outlet switching of Lake Agassiz drainage (Clark et al., 2001; Teller and Leverington, 2004).

We also find that a NW outlet for Lake Agassiz was very likely active from no later than −11.9 to −10.8 ka. Drainage of Lake Agassiz/Ojibway into the Arctic ocean was also likely during much of the −9.2 to −8.5 ka interval. With the margin chronology employed (Dyke, 2004), the SO is permanently closed after YD onset. However, blockage of NW drainage by a short-termed re-advance of ice in western Manitoba around −11.4 ka (Thorleifson, 1996) offers a possible reconciliation of evidence for a NW outburst flood at −11.3 ka along with evidence for a brief occupation of the SO that ^{14}C dates indicate occurred some time after −11.5 ka and before −10.6 ka. Another option for obtaining a southern drainage event that is possibly consistent with the model is an ice blockage of NW drainage during the upper Campbell stage at −10.7 ka.

The reconstructed order 1.5–2.0 dSv (including precipitation over ice-free land) outflows into both the eastern North Atlantic and Gulf of Mexico during the B–A support the lower sensitivity of the THC to these regions of meltwater injection. This is most probably a consequence of turbulent mixing in the Gulf Stream (due to high baroclinic instability) along with the sediment-laden nature of the outflows which caused them to be hyperpycnal bottom-riding flows rather than a mass of surface-riding freshwater that would be expected to have caused significant impact upon the THC.

The validity of our new drainage chronology rests in part on the accuracy of the new margin forcing chronology of Dyke (2004). The relatively close correspondence of model results with a host of proxy data lends validity to both the results themselves as well as to the most critical features of the margin chronology. Further testing of our NW YD trigger hypothesis will require collection and analysis of $\delta^{18}O$ records for the Beaufort Sea, field-based verification of the drainage chronology around the Clearwater Athabasca spillway and Wapawekka Hills (NW choke-point) regions, refinement of the margin chronology, incorporation of a relatively large set of strandline data into the model calibration, as well as similar modelling analyses and observational data (e.g., Spielhagen et al., 2005; Jennings et al., 2006) to constrain Eurasian and Greenland meltwater drainage chronologies.

Acknowledgements

This paper is a contribution to the Polar Climate Stability Research Network that is funded by the Canadian Foundation for Climate and Atmospheric Sciences and a consortium of Canadian universities. Additional support for the work has been provided by NSERC Grant A9627. We are especially grateful to Art Dyke, Tim Fisher, Claude Hillaire-Marcel, and Jim Teller for helpful discussions. GRIP and GISP II Data were provided by the National Snow and Ice Data Center, University of Colorado at Boulder, and the WDC-A for Paleoclimatology, National Geophysical Data Center, Boulder, Colorado.

One of us (W. R. P.) wishes to thank both Wally Broecker and Gary Comer for enabling him to participate in a field trip to the Fort McMurray area of Alberta during which we were able to overfly one of the main channels through which Agassiz water was routed to the sea.

References

Aagaard, K., Carmack, E.C., 1989. The role of sea ice and other fresh water in the Arctic Circulation. Journal of Geophysical Research 94 (C10), 14485–14498.

Aharon, P., 2003. Meltwater flooding events in the Gulf of Mexico revisited: implications for rapid climate changes during the last deglaciation. Paleoceanography 18 (4), 1079.

Aharon, P., 2006. Entrainment of meltwaters in hyperpycnal flows during deglaciation superfloods in the Gulf of Mexico. Earth and Planetary Science Letters 241 (1–2): 260–272.

Barber, D.C., Dyke, A., Hillaire-Marcel, C., Jennings, A.E., Andrews, J.T., Kerwin, M.W., Bilodeau, G., McNeely, R., Southon, J., Morehead, M.D., Gagnon, J.-M., 1999. Forcing of the cold event 8200 years ago by outburst drainage of Laurentide lakes. Nature 400, 344–348.

Bauch, H.A., Erlenkeuser, H., Spielhagen, R.F., Matthiessen, U.S.J., Thiede, J., Heinemeier, J., 2001. A multiproxy reconstruction of the evolution of deep and surface waters in the subarctic Nordic seas over the last 30,000 yr. Quaternary Science Reviews 20, 659–678.

Blais-Stevens, A., Clague, J.J., Mathewes, R.W., Hebda, R.J., Bornhold, B.D., 2003. Record of large, Late Pleistocene outburst floods preserved in Saanich Inlet sediments, Vancouver Island, Canada. Quaternary Science Reviews 22, 2327–2334.

Broecker, W.S., Kennett, J.P., Flower, B.P., Teller, J.T., Trumbore, S., Bonani, G., Wolfli, W., 1989. Routing of meltwater from the Laurentide Ice Sheet during the Younger Dryas cold episode. Nature 341 (6240), 318–321.

Brown, P.A., Kennett, J.P., 1998. Megaflood erosion and meltwater plumbing changes during last North American deglaciation recorded in Gulf of Mexico sediments. Geology 26 (7), 599–602.

Budd, W.F., Smith, I.N., 1981. The growth and retreat of ice sheets in response to orbital radiation changes. In: Sea Level, Ice and Climatic Changes, vol. 131. International Association of Hydrological Science, pp. 369–409.

Bush, A.B., McWilliams, J.C., Peltier, W.R., 1996. The formation of oceanic eddies in symmetric and asymmetric jets. Part II, late time

evolution and coherent vortex formation. Journal of Physical Oceanography 26 (9), 1825–1848.
Clark, P., Alley, R., Keigwin, L., Licciardi, J., Johnsen, S., Wang, H., 1996. Origin of the first global meltwater pulse following the last glacial maximum. Paleoceanography 11 (5), 563–577.
Clark, P.U., Marshall, S.J., Clarke, G.K., Hostetler, S.W., Licciardi, J.M., Teller, J.T., 2001. Freshwater forcing of abrupt climate change during the last glaciation. Science 293 (5528), 283–287.
Clark, P.U., Mitrovica, J.X., Milne, G.A., Tamisiea, M.E., 2002. Sea-level fingerprinting as a direct test for the source of global meltwater pulse 1a. Science 295, 2438–2441.
Clarke, G.K.C., Leverington, D.W., Teller, J.T., Dyke, A.S., 2004. Paleohydraulics of the last outburst flood from glacial Lake Agassiz and the 8200 BP cold event. Quaternary Science Reviews 23 (3–4), 389–407.
Cofaigh, C.O., Dowdeswell, J.A., 2001. Late Quaternary iceberg rafting along the Antarctic Peninsula Continental Rise and in the Weddell and Scotia Seas. Quaternary Research 56, 308–321.
Colman, S.M., Clark, J., Clayton, L., Hansel, A.K., Larsen, C.E., 1994a. Deglaciation, lake levels, and meltwater discharge in the Lake Michigan basin. Quaternary Science Reviews 13, 879–890.
Colman, S.M., Keigwin, L.D., Forester, R.M., 1994b. 2 episodes of meltwater influx from glacial Lake Agassiz into the Lake-Michigan basin and their climatic contrasts. Geology 22 (6), 547–550.
Conway, H., Hall, B.L., Denton, G.H., Gades, A.M., Waddington, E.E., 1999. Past and future grounding-line retreat of the West Antarctic Ice Sheet. Science 286 (5438), 280–283.
de Vernal, A., Hillaire-Marcel, C., Bilodeau, G., 1996. Reduced meltwater outflow from the Laurentide ice margin during the Younger Dryas. Nature 381 (6581), 774–777.
Denton, G.H., Hughes, T.J., 2002. Reconstructing the Antarctic Ice Sheet at the Last Glacial Maximum. Quaternary Science Reviews 21 (1–3), 193–202.
Dyke, A.S., 2004. An outline of North American deglaciation with emphasis on central and northern Canada. In: Ehlers, J., Gibbard, P.L. (Eds.), Quaternary Glaciations—Extent and Chronology, Part II, vol. 2b. Elsevier, Amsterdam, pp. 373–424.
Dyke, A.S., Prest, V.K., 1987. Late Wisconsinan and Holocene history of the Laurentide ice sheet. Geographie Physique et Quaternaire 41, 237–264.
Dyke, A.S., Savelle, J.M., 2000. Major end moraines of Younger Dryas age on Wollaston Peninsula, Victoria Island, Canadian Arctic: implications for paleoclimate and for formation of hummocky moraines. Canadian Journal of Earth Sciences 37 (4), 601–619.
Dyke, A.S., Andrews, J.T., Clark, P.U., England, J.H., Miller, G.H., Shaw, J., Veillette, J., 2002. The Laurentide and Innuitian ice sheets during the Last Glacial Maximum. Quaternary Science Reviews 21, 9–31.
Dyke, A.S., Moore, A., Robertson, L., 2003. Deglaciation of North America. Technical Report Open File 1574, Geological Survey of Canada, thirty-two maps at 1:7 000 000 scale with accompanying digital chronological database and one poster (in two sheets) with full map series.
Dziewonski, A.M., Anderson, D.L., 1981. Preliminary reference Earth model. Physics of the Earth and Planetary Interiors 25, 297–356.
Fairbanks, R.G., 1989. A 17,000-year glacio-eustatic sea level record: influence of glacial melting rates on the Younger Dryas event and deep-ocean circulation. Nature 342, 637–641.
Fenton, M.M., Moran, S.R., Teller, J.T., Clayton, L., 1983. Quaternary stratigraphy and history in the southern part of the Lake Agassiz basin. In: Teller, J.T., Clayton, L. (Eds.), Glacial Lake Agassiz, Special Paper 26. Geological Association of Canada, St. John's, Newfoundland, pp. 49–74.
Fisher, T.G., 2003. Chronology of glacial Lake Agassiz meltwater routed to the Gulf of Mexico. Quaternary Research 59 (2), 271–276.
Fisher, T.G., 2005a. Abandonment chronology of glacial Lake Agassiz's northwestern outlet. Palaeogeography Palaeoclimatology Palaeoecology, in press.
Fisher, T.G., 2005. Strandline analysis in the southern basin of glacial Lake Agassiz Minnesota and North and South Dakota, USA. Geological Society of America Bulletin 117 (11/12), 1481–1496.
Fisher, T.G., Smith, D.G., 1994. Glacial Lake Agassiz—its northwest maximum extent and outlet in Saskatchewan (Emerson phase). Quaternary Science Reviews 13 (9–10), 845–858.
Fisher, T.G., Souch, C., 1998. Northwest outlet channels of Lake Agassiz isostatic tilting and a migrating continental drainage divide, Saskatchewan, Canada. Geomorphology 25, 57–73.
Fisher, T.G., Smith, D.G., Andrews, J.T., 2002. Preboreal oscillation caused by a glacial Lake Agassiz flood. Quaternary Science Reviews 21, 873–878.
Fulton, R.J., 1995. Surficial materials of Canada. Geological Survey of Canada, Map 1880A, scale 1:5000000, online.
Hanebuth, T., Stattegger, K., Grootes, P.M., 2000. Rapid flooding of the Sunda Shelf: a late glacial sea level record. Science 288 (5468), 1033–1035.
Hemming, S.R., 2004. Massive late pleistocene detritus layers of the North Atlantic and their global climate imprint. Reviews of Geophysics 42 (RG1005).
Hughen, K.A., Overpeck, J.T., Lehman, S.J., Kashgarian, M., Southon, J., Petersonk, L.C., Alley, R., Sigman, D.M., 1998. Deglacial changes in ocean circulation from an extended radiocarbon calibration. Nature 391, 65–68.
Huybrechts, P., 2002. Sea-level changes at the LGM from ice-dynamic reconstructions of the Greenland and Antarctic ice sheets during the glacial cycles. Quaternary Science Reviews 21 (1–3), 203–231.
Imbrie, J., Hays, J.D., Martinson, D., McIntyre, A., Mix, A.C., Morley, J.J., Pisias, N.G., Prell, W.L., Shackleton, N.J., 1984. The orbital theory of Pleistocene climate: support from a revised chronology of the marine δ^{18}O record. In: Berger, A., Imbrie, J., Hays, H., Kukla, G., Saltzman, B. (Eds.), Milankovitch and Climate: Understanding the Response to Astronomical Forcing. NATO ASI Series. Series C, Mathematical and Physical Sciences, vol. 126. D. Reidel, Dordrecht, pp. 269–305.
Jennings, A.E., Hald, M., Smith, M., Andrews, J.T., 2006. Freshwater forcing from the Greenland ice sheet during the Younger Dryas: evidence from southeastern Greenland shelf cores. Quaternary Science Reviews 25, 282–298.
Jenson, J.W., MacAyeal, D.R., Clark, P.U., Ho, C.L., Vela, J.C., 1996. Numerical modeling of subglacial sediment deformation: implications for the behaviour of the Lake Michigan Lobe, Laurentide Ice Sheet. Journal of Geophysical Research 101 (B4), 8717–8728.
Johnsen, S.J., Dansgaard, W., White, J.W.C., 1989. The origin of Arctic precipitation under present and glacial conditions. Tellus 41, 452–469.
Johnsen, S.J., Dahl-Jensen, D., Gundestrup, N., Steffensen, J.P., Clausen, H.B., Miller, H., Masson-Delmotte, V., Sveinbjornsdottir, A.E., White, J., 2001. Oxygen isotope and palaeotemperature records from six Greenland ice-core stations: Camp Century, Dye-3, GRIP, GISP2, Renland and NorthGRIP. Journal of Quaternary Science 16, 299–307.
Kalnay, E., Kanamitsu, M., Kistler, R., Collins, W., Deaven, D., Gandin, L., Iredell, M., Saha, S., White, G., Woollen, J., Zhu, Y., Leetmaa, A., Reynolds, B., Chelliah, M., Ebisuzaki, W., Higgins, W., Janowiak, J., Mo, K., Ropelewski, C., Wang, J., Jenne, R., Joseph, D., 1996. The NCEP/NCAR 40-year reanalysis project. Bulletin of the American Meteorological Society 77, 437–471.
Karrow, 2002. Correspondence: comment on "Formation of large beaches in an area of rapid differential isostatic rebound: the three-outlet control of Lake Agassiz" by J.T. Teller. Quaternary Science Reviews 21, 2115–2118.
Keigwin, L.D., Jones, J.A., Lehman, S.J., Boyle, E.A., 1991. Deglacial meltwater discharge North-Atlantic deep circulation, and abrupt climate change. Journal of Geophysical Research 96 (C9), 16811–16826.
Kirby, M.E., 1998. Heinrich event-0 (DC-0) in sediment cores from the northwest Labrador in Cumberland Sound: recording events in Cumberland Sound? Canadian Journal of Earth Sciences 35, 510–519.

Lambert, A., Courtier, N., Sasegawa, G.S., Klopping, F., Winester, D., James, T., Liard, J.O., 2001. New constraints on Laurentide postglacial rebound from absolute gravity measurements. Geophysical Research Letters 28, 2109–2112.

Laske, G., Masters, G., 1997. A global digital map of sediment thickness. EOS Transactions 78, F483.

Legates, D.R., Willmott, C.J., 1990. Mean seasonal and spatial variability in gauge-corrected global precipitation. International Journal of Climatology 10 (2), 111–127.

Leverington, D.W., Mann, J.D., Teller, J.T., 2002. Changes in the bathymetry and volume of glacial Lake Agassiz. Quaternary Science Reviews 57, 244–252.

Licciardi, J.M., Teller, J.T., Clark, P.U., 1999. Freshwater routing by the Laurentide Ice Sheet during the last deglaciation. In: Clark, P.U., Webb, R.S., Keigwin, L.D. (Eds.), Mechanisms of Global Climate Change at Millennial Time Scales. Geophysical Monographs, vol. 112. AGU, pp. 177–201.

Lohmann, G., Schulz, M., 2000. Reconciling Bolling warmth with peak deglacial meltwater discharge. Paleoceanography 15 (5), 537–540.

Lowell, T.V., Fisher, T.G., Comer, G., Hajdas, I., Waterson, N., Glover, K., Loope, H., Schaefer, J., Rinterknecht, V., Broecker, W., Denton, G., Teller, J., 2005. Testing the Lake Agassiz Meltwater Trigger for the Younger Dryas. EOS 86 (40), 365–373.

Manabe, S., Stouffer, R.J., 1997. Coupled ocean–atmosphere model response to freshwater input: comparison to Younger Dryas event. Paleoceanography 12, 321–336.

Marchitto, T.M., Wei, K.Y., 1995. History of Laurentide meltwater flow to the Gulf-of-Mexico during the last deglaciation, as revealed by reworked calcareous nanofossils. Geology 23 (9), 779–782.

Marshall, S.J., Clarke, G.K.C., 1999. Modeling North American freshwater runoff through the last glacial cycle. Quaternary Research 52, 300–315.

McManus, J.F., Francois, R., Gherardi, J.-M., Keigwin, L.D., Brown-Leger, S., 2004. Collapse and rapid resumption of Atlantic meridional circulation linked to deglacial climate changes. Nature 428 (6985), 834–837.

Minning, G.V., Cowan, W.R., Sharpe, D.R., Warmann, T.A., 1994. Quaternary geology and drift composition, Lake of the Woods region, northwestern Ontario. Technical Report Memoir 436, Geological Survey of Canada, 239pp.

Muscheler, R., Beer, J., Wagner, G., Finkel, R., 2000. Changes in deep-water formation during the Younger Dryas event inferred from ^{10}Be and ^{14}C records. Nature 408, 467–570.

Norgaard-Pedersen, N., Spielhagen, R.F., Erlenkeuser, H., Grootes, P.M., Heinemeier, J., Knies, J., 2003. Arctic Ocean during the Last Glacial Maximum: Atlantic and polar domains of surface water mass distribution and ice cover. Paleoceanography 18 (3).

Oppenheimer, M., 1998. Global warming and the stability of the West Antarctic Ice Sheet. Nature 393, 325–332.

Parsons, J.D., Bush, J.W., Syvitski, J.P., 2001. Hyperpycnal plume formation from riverine outflows with small sediment concentrations. Sedimentology 48, 465–478.

Payne, A.J., Huybrechts, P., Abe-Ouchi, A., Calov, R., Fastook, J., Greve, R., Marshall, S.J., Marsiat, I., Ritz, C., Tarasov, L., Thomassen, M., 2000. Results from the EISMINT model intercomparison: the effects of thermomechanical coupling. Journal of Glaciology 46 (153), 227–238.

Peltier, W.R., 1974. The impulse response of a Maxwell Earth. Reviews of Geophysics 12, 649–669.

Peltier, W.R., 1976. Glacial isostatic adjustment II: the inverse problem. Geophysical Journal of the Royal Astronomical Society 46, 669–706.

Peltier, W.R., 1994. Ice age paleotopography. Science 265, 195–201.

Peltier, W.R., 1996. Mantle viscosity and ice age ice sheet topography. Science 273, 1359–1364.

Peltier, W.R., 1998. Postglacial variations in the level of the sea: implications for climate dynamics and solid-earth geophysics. Reviews of Geophysics 36, 603–689.

Peltier, W.R., 2002. Global glacial isostatic adjustment: Paleo-geodetic and space-geodetic tests of the ICE-4G VM2 model. Journal of Quaternary Science 17 (5–6), 491–510.

Peltier, W.R., 2004. Global glacial isostatic adjustment and the surface of the ice-age Earth: the ICE-5G (VM2) model and GRACE. Annual Review of Earth and Planetary Sciences 32, 111–149.

Peltier, W.R., 2005. On the hemispheric origins of meltwater pulse 1a. Quaternary Science Reviews 24 (14–15), 1655–1671.

Peltier, W.R., Jiang, X., 1996. Mantle viscosity from the simultaneous inversion of multiple data sets pertaining to postglacial rebound. Geophysical Research Letters 23, 503–506.

Pollack, H.N., Hurter, S.J., Johnson, J.R., 1993. Heat flow from the Earth's interior: analysis of the global data set. Reviews of Geophysics 31, 267–280.

Poore, R.Z., Osterman, L., Curry, W.B., Phillips, R.L., 1999. Late Pleistocene and Holocene meltwater events in the western Arctic Ocean. Geology 27 (8), 759–762.

Rayburn, J.A., 1997. Correlation of the Campbell strandlines along the northwestern margin of Glacial Lake Agassiz. M.Sc. Thesis, University of Manitoba.

Reimer, P.J., Baillie, M.G., Bard, E., Bayliss, A., Beck, J.W., Bertrand, C., Blackwell, P.G., Buck, C.E., Burr, G., Cutler, K.B., Damon, P.E., Edwards, R.L., Fairbanks, R.G., Friedrich, M., Guilderson, T.P., Hughen, K.A., Kromer, B., McCormac, F.G., Manning, S., Ramsey, C.B., Reimer, R.W., Remmele, S., Southon, J.R., Stuiver, M., Talamo, S., Taylor, F.W., van der Plicht, J., Weyhenmeyer, C.E., 2004. IntCal04 Terrestrial radiocarbon age calibration, 26—0 ka BP. Radiocarbon 46, 1029–1058.

Rennick, M., 1977. The parameterization of tropospheric lapse rates in terms of surface temperature. Journal of the Atmospheric Sciences 34, 854–862.

Richard, P.J., Occhietti, S., 2005. ^{14}C chronology for ice retreat and inception of Champlain Sea in the St. Lawrence Lowlands. Canada: Quaternary Research 63 (3), 353–358.

Rodrigues, C.G., Vilks, G., 1994. The impact of glacial lake runoff on the Goldthwait and Champlain Seas: the relationship between glacial Lake Agassiz runoff and the Younger Dryas. Quaternary Science Reviews 13, 923–944.

Rooth, C., 1982. Hydrology and ocean circulation. Progress in Oceanography 7, 131–149.

Saarnisto, M., Lunkka, J.P., 2005. Climate variability during the last interglacial-glacial cycle in NW Eurasia. In: Battarbee, R.W., Gasse, F., Stickley, C.E. (Eds.), Past Climate Variability through Europe and Africa, Developments in Paleoenvironmental Research, vol. 6. Kluwer, Dordrecht (Chapter 21).

Schreiner, B.T., 1983. Lake Agassiz in Saskatchewan. In: Teller, J.T., Clayton, L. (Eds.), Glacial Lake Agassiz. Special Paper 26. Geological Association of Canada, St. John's, Newfoundland, pp. 49–74.

Smith, D.G., 1994. Glacial Lake McConnell: paleogeography, age, duration, and associated river deltas, Mackenzie River basin, Western Canada. Quaternary Science Reviews 13, 829–843.

Smith, D.G., Fisher, T.G., 1993. Glacial Lake Agassiz: the northwest outlet and paleoflood. Geology 21, 9–12.

Spielhagen, R.F., Erlenkeuser, H., Siegert, C., 2005. History of freshwater runoff across the Laptev Sea (Arctic) during the last deglaciation. Global and Planetary Change 48, 187–207.

Stoner, J.S., Channell, J.E.T, Hillaire-Marcel, C., 1996. The magnetic signature of rapidly deposited detrital layers from the deep Labrador Sea: relationship to North Atlantic Heinrich layers. Paleoceanography 11, 309–325.

Stuiver, M., Reimer, P.J., 1993. Extended 14C database and revised CALIB radiocarbon calibration program. Radiocarbon 35, 215–230.

Stuiver, M., Reimer, P.J., Bard, E., Beck, W., Burr, G.S., Hugen, K.A., Kromer, B., McCormac, G., van der Plicht, J., Spurk, M., 1998a. INTCAL98 radiocarbon age calibration 24,000-0 cal BP. Radiocarbon 40, 1041–1084.

Stuiver, M., Reimer, P.J., Braziunas, T.F., 1998b. High-precision radiocarbon age calibration for terrestrial and marine samples. Radiocarbon 40, 1127–1151.

Tarasov, L., Peltier, W.R., 1997. Terminating the 100 kyr ice age cycle. Journal of Geophysical Research 102 (D18), 21665–21693.

Tarasov, L., Peltier, W.R., 1999. Impact of thermomechanical ice sheet coupling on a model of the 100 kyr ice age cycle. Journal of Geophysical Research 104, 9517–9545.

Tarasov, L., Peltier, W.R., 2002. Greenland glacial history and local geodynamic consequences. Geophysical Journal International 150, 198–229.

Tarasov, L., Peltier, W.R., 2003. Greenland glacial history, borehole constraints and Eemian extent. Journal of Geophysical Research 108 (B3), 2124–2143.

Tarasov, L., Peltier, W.R., 2004. A geophysically constrained large ensemble analysis of the deglacial history of the North American ice sheet complex. Quaternary Science Reviews 23, 359–388.

Tarasov, L., Peltier, W.R., 2005. Arctic freshwater forcing of the Younger Dryas cold reversal. Nature 435, 662–665.

Teller, J.T., 2001. Formation of large beaches in an area of rapid differential isostatic rebound: the three-outlet control of Lake Agassiz. Quaternary Science Reviews 20, 1649–1659.

Teller, J.T., 2002. Correspondence, reply to the comment by P.F. Karrow. Quaternary Science Reviews 21, 2119–2122.

Teller, J.T., Leverington, D.W., 2004. Glacial Lake Agassiz: a 5000 yr history of change and its relationship to the δ^{18}O record of Greenland. GSA Bulletin 116 (5/6), 729–742.

Teller, J.T., Thorleifson, L.H., 1983. The Lake Agassiz–Lake Superior connection. In: Teller, J.T., Clayton, L. (Eds.), Glacial Lake Agassiz. Special Paper 26. Geological Association of Canada, St. John's, Newfoundland, pp. 261–290.

Teller, J.T., Risberg, J., Matile, G., Zoltai, S., 2000. Postglacial history and paleoecology of Wampum, Manitoba, a former lagoon in the Lake Agassiz basin. Geological Society of America Bulletin 112 (6), 943–958.

Teller, J.T., Leverington, D.W., Mann, J.D., 2002. Freshwater outbursts to the oceans from glacial Lake Agassiz and their role in climate change during the last deglaciation. Quaternary Science Reviews 21, 879–887.

Teller, J.T., Boyd, M., Yang, Z., Kor, P.S.G., Fard, A.M., 2005. Alternative routing of Lake Agassiz overflow during the Younger Dryas: new dates, paleotopography, and a reevaluation. Quaternary Science Reviews 24, 1890–1905.

Thorleifson, L.H., 1996. Review of Lake Agassiz history, in: Teller, J., Thorleifson, L.H., Matile, G., Brisbin, W.C. (Eds.), Sedimentology, Geomorphology, and History of the Central Lake Agassiz basin, Field Trip Guidebook, vol. B2. Geological Association of Canada Annual Meeting, pp. 55–94.

Vinje, T., Nordlund, N., Kvambekk, A., 1998. Monitoring ice thickness in Fram Strait. Journal of Geophysical Research 103 (C5), 10437–10449.

Weaver, A.J., Saenko, O.A., Clark, P.U., Mitrovica, J.X., 2003. Meltwater pulse 1A from Antarctica as a trigger of the Bolling–Allerod warm interval. Science 299, 1709–1713.

Yansa, C.H., Ashworth, A.C., 2005. Late Pleistocene palaeoenvironments of the southern Lake Agassiz Basin, USA. Quaternary Science 20 (3), 255–267.